Received: 22 March 2020 | Revised: 12 June 2020 | Accepted: 19 June 2020

DOI: 10.1096/fj.202000678R

RESEARCH ARTICLE

THE FASEB JOURNAL

Liver CPT1A gene therapy reduces diet-induced hepatic steatosis in mice and highlights potential lipid biomarkers for human NAFLD

Minéia Weber[1] | Paula Mera[1,2] | Josefina Casas[3,4] | Javier Salvador[2,5] | Amaia Rodríguez[2,6] | Sergio Alonso[7] | David Sebastián[8,9] | M. Carmen Soler-Vázquez[1] | Carla Montironi[10,11] | Sandra Recalde[1] | Raquel Fucho[1] | María Calderón-Domínguez[1] | Joan Francesc Mir[1] | Ramon Bartrons[12] | Joan Carles Escola-Gil[13,9] | David Sánchez-Infantes[14,2] | Antonio Zorzano[8,9] | Vicenta Llorente-Cortes[15,16,17] | Núria Casals[18,2] | Víctor Valentí[6,19] | Gema Frühbeck[2,6] | Laura Herrero[1,2] | Dolors Serra[1,2]

[1]Department of Biochemistry and Physiology, School of Pharmacy and Food Sciences, Institut de Biomedicina de la Universitat de Barcelona (IBUB), Universitat de Barcelona, Barcelona, Spain

[2]Centro de Investigación Biomédica en Red de Fisiopatología de la Obesidad y la Nutrición (CIBEROBN), Instituto de Salud Carlos III, Madrid, Spain

[3]Research Unit on BioActive Molecules, Department of Biological Chemistry, Institute of Advanced Chemistry of Catalonia (IQAC)/CSIC, Barcelona, Spain

[4]Centro de Investigación Biomédica en Red de Enfermedades Hepáticas y Digestivas (CIBEREHD), Instituto de Salud Carlos III, Madrid, Spain

[5]Department of Endocrinology & Nutrition, Clínica Universidad de Navarra, Pamplona, Spain

[6]Metabolic Research Laboratory, Clínica Universidad de Navarra, IdiSNA, Pamplona, Spain

[7]Cancer Genetics and Epigenetics Group, Program of Predictive and Personalized Medicine of Cancer, Germans Trias i Pujol Research Institute (IGTP-PMPPC), Campus Can Ruti, Barcelona, Spain

[8]Institute for Research in Biomedicine (IRB Barcelona), Barcelona Institute of Science and Technology, Departament de Bioquímica i Biomedicina Molecular, Facultat de Biologia, Universitat de Barcelona, Barcelona, Spain

[9]Centro de Investigación Biomédica en Red de Diabetes y Enfermedades Metabólicas Asociadas (CIBERDEM), Instituto de Salud Carlos III, Madrid, Spain

[10]Pathology Department, Hospital Clinic de Barcelona, Barcelona, Spain

[11]Liver Cancer Translational Research Laboratory, Liver Unit, IDIBAPS-Hospital Clínic, Universitat de Barcelona, Barcelona, Spain

[12]Departament de Ciències Fisiològiques, Facultat de Medicina i Ciències de la Salut, Universitat de Barcelona, Spain

[13]IIB Sant Pau, Departament de Bioquímica i Biologia Molecular, Universitat Autònoma de Barcelona, Barcelona, Spain

[14]Germans Trias i Pujol Research Institute (IGTP-PMPPC), Campus Can Ruti, Barcelona, Spain

[15]Institute of Biomedical Research of Barcelona (IIBB), Spanish National Research Council (CSIC), Biomedical Research Institute Sant Pau (IIB Sant Pau), Barcelona, Spain

[16]CIBERCV, Institute of Health Carlos III, Madrid, Spain

[17]Cardiovascular Research Center, CSIC-ICCC, Barcelona, Spain

[18]Basic Sciences Department, Faculty of Medicine and Health Sciences, Universitat Internacional de Catalunya, Sant Cugat del Vallès, Spain

Abbreviations: AAV, adeno-associated viruses; ACC1, acetyl-CoA carboxylase 1; ASP, acid-soluble products; BHB-CoA, β-hydroxybutyryl-CoA; CPT1A, carnitine palmitoyltransferase 1A; DAG, diacylglycerides; DGAT2, diacylglycerol O-acyltransferase homolog 2; FA, fatty acids; FFA, free fatty acid; FAO, fatty acid oxidation; GFP, green fluorescent protein; G6Pase, glucose-6-phosphatase; GTT, glucose tolerance test; HFD, high-fat diet; HMGCS2, hydroxymethylglutaryl-CoA synthase 2; IR, insulin resistance; LPE, lysophosphatidylethanolamine; MCD, malonyl-CoA decarboxylase; MTP, microsomal triacylglycerol transfer protein; NAFLD, nonalcoholic fatty liver disease; NAS, NAFLD activity score; qRT-PCR, real-time quantitative PCR; PC, phosphatidylcholine; ROS, reactive oxygen species; RYGB, Roux-en-Y gastric bypass; TAG, triacylglyceride; UCP2, uncoupling protein 2; VLDL, very-low-density lipoprotein.

Minéia Weber and Paula Mera contributed equally to this study.

[19]Department of Surgery, Clínica Universidad de Navarra, Pamplona, Spain

Correspondence
Dolors Serra, Department of Biochemistry and Physiology, School of Pharmacy and Food Sciences, University of Barcelona, Av. Joan XXIII, 27-31, E-08028 Barcelona, Spain.
Email: dserra@ub.edu

Funding information
Ministry of Spain (MINECO), Grant/Award Number: SAF2014-52223-C2-1-R, and SAF2017-83813-C3-1-R; European Regional Development Fund [ERDF; Juan de la Cierva—Incorporación, Grant/Award Number: IJCI-2016-28313; Centro de Investigación Biomédica en Red de Fisiopatología de la Obesidad y la Nutrición (CIBEROBN), Grant/Award Number: CB06/03/0001; Government of Catalonia, Grant/Award Number: 2014SGR465; Instituto de Salud Carlos III, Grant/Award Number: FISPI18/01584, FIS-PI17/00412, FIS PI18/01484, FIS17/01455, CP15/00106, CM19/00039 ; European Regional Development Fund (ERDF); Fundació La Marató de TV3, Grant/Award Number: 201627-30, 201627-31; European Foundation for the Study of Diabetes (EFSD); Lilly; Janssen-Rising Star; L'Oréal-UNESCO; Ciência sem Fronteiras-CNPq, Grant/Award Number: 237976/2012-9

Abstract

The prevalence of nonalcoholic fatty liver disease (NAFLD) has increased drastically due to the global obesity pandemic but at present there are no approved therapies. Here, we aimed to revert high-fat diet (HFD)-induced obesity and NAFLD in mice by enhancing liver fatty acid oxidation (FAO). Moreover, we searched for potential new lipid biomarkers for monitoring liver steatosis in humans. We used adeno-associated virus (AAV) to deliver a permanently active mutant form of human carnitine palmitoyltransferase 1A (hCPT1AM), the key enzyme in FAO, in the liver of a mouse model of HFD-induced obesity and NAFLD. Expression of hCPT1AM enhanced hepatic FAO and autophagy, reduced liver steatosis, and improved glucose homeostasis. Lipidomic analysis in mice and humans before and after therapeutic interventions, such as hepatic AAV9-hCPT1AM administration and RYGB surgery, respectively, led to the identification of specific triacylglyceride (TAG) specie (C50:1) as a potential biomarker to monitor NAFFLD disease. To sum up, here we show for the first time that liver hCPT1AM gene therapy in a mouse model of established obesity, diabetes, and NAFLD can reduce HFD-induced derangements. Moreover, our study highlights TAG (C50:1) as a potential noninvasive biomarker that might be useful to monitor NAFLD in mice and humans.

KEYWORDS
AAV, CPT1A, fatty-acid oxidation, gene therapy, hepatic steatosis, lipid biomarker, obesity

1 | INTRODUCTION

Despite enormous efforts by health-care providers and the research community, obesity rates continue to rise. Unfortunately, safe, long-term efficient treatments are currently unavailable. Of great concern is the parallel increase in the prevalence of obesity-associated pathological conditions such as insulin resistance, type 2 diabetes (T2D), nonalcoholic fatty liver disease (NAFLD), cardiovascular disease, and cancer. Hence, it is vital to develop novel therapeutic strategies to combat this epidemic.

One of the main causes of obesity is the modern lifestyle, which is characterized by excessive calorie intake and insufficient physical activity. The liver plays an essential role in regulating whole-body energy balance and lipid/glucose homeostasis. In conditions associated with prolonged excess energy intake, the liver can store significant quantities of lipids, which eventually leads to steatosis. Liver steatosis can cause hepatic inflammation and progress to steatohepatitis (NASH),[1] which predisposes to hepatic injury and cancer. The design of new therapeutic strategies to enhance fat burning in liver may alleviate these obesity-related disorders.

Mitochondrial long-chain fatty acid β-oxidation (FAO) is regulated by carnitine palmitoyltransferase 1 (CPT1). This enzyme is physiologically inhibited by malonyl-CoA, a glucose-derived metabolite that is an intermediate in the de novo synthesis of fatty acids (FA). Increased glucose metabolism raises levels of malonyl-CoA, which inhibits CPT1 and blocks FAO, resulting in lipid partitioning and storage. A significant number of studies in rodents have tried to indirectly promote FAO to reduce systemic obesity and prevent the development of obesity-associated metabolic disorders. These studies targeted the regulation of enzymes and transcription factors involved in FA metabolism, such as acetyl-CoA carboxylase (ACC),[2] malonyl-CoA decarboxylase (MCD),[3] uncoupling protein 1 (UCP1),[4] AMP-activated protein kinase (AMPK),[5] peroxisome proliferator-activated receptor (PPAR),[6] and long-chain acyl-CoA dehydrogenase (VLCAD).[7] Studies that increased short-term CPT1A activity in liver demonstrated a decrease in hepatic triglyceride (TAG) content,[8] but did not report any improvement in insulin sensitivity. Furthermore, we and others have shown that a long-term increase in CPT1A and a mutated isoform that is insensitive to malonyl-CoA (CPT1AM)[9] prevented steatosis and the development of obesity in mice fed a high-fat diet (HFD).[10,11] Still, these studies could not revert the HFD-induced derangements in an established model of obesity.

The aim of the present study was to determine whether AAV-mediated long-term activation of hepatic FAO could be a successful strategy to revert an already established obesity with associated hyperglycemia and NAFLD in mice. We focused on three novel strategies: (1) use of the AAV9 serotype, which is the most effective AAV in gene therapy at targeting liver; (2) use of a mouse model with established obesity, type 2 diabetes, and NAFLD; and (3) use of the human isoform of CPT1AM (hCPT1AM), with the prospect of future clinical therapeutic applications. Our results show that enhanced hepatic FAO through hCPT1AM-mediated gene therapy reduces diet-induced weight gain, and hepatic steatosis and improves hepatic insulin signaling in obese mice. Mechanistically, hCPT1AM-expressing mice showed enhanced autophagy, ketogenesis, and oxidative phosphorylation in the liver. Importantly, hCPT1AM expression also changes the hepatic lipidomic profile. One of the altered lipid species, C50:1 triacylglyceride, was concomitantly lower in the serum of human patients with obesity and NAFLD after bariatric surgery. Thus, we identified a potential biomarker to monitor the progression of hepatic steatosis in humans.

2 | MATERIALS AND METHODS

2.1 | Human study cohort and biological analysis

Serum samples were obtained from obese patients (BMI ≥ 30 kg/m^2 and body fat percentage [BF] ≥35% for women and ≥ 25% for men) before and 6 months after Roux-en-Y gastric bypass (RYGB) (n = 15) and from healthy lean volunteers (n = 15) at the *Clínica Universidad de Navarra*. Inclusion criteria included a complete diagnosis: physical examination, laboratory investigation, ultrasound echography, and a liver biopsy consistent with the diagnosis of nonalcoholic fatty liver disease (NAFLD), according to Brunt criteria.[12] Exclusion criteria were: (i) excess alcohol consumption (≥20 g for women and ≥30 g for men); (ii) the presence of hepatitis B virus surface antigen or hepatitis C virus antibodies in the absence of a history of vaccination; (iii) use of drugs linked to NAFLD, including amiodarone, valproate, tamoxifen, methotrexate, corticosteroids, or antiretrovirals; (iv) evidence of other specific liver diseases, such as autoimmune liver disease, hemochromatosis, Wilson's disease, or α-1-antitrypsin deficiency. Patients with type 2 diabetes (T2D) were not on any antidiabetic treatment before or during the study. Obese patients with T2D did not have a long history of diabetes (less than 2-3 years or even de novo diagnosis as evidenced from their anamnesis and biochemical determinations). Glucose, uric acid, ALT, AST, alkaline phosphatase, and γ-glutamyltransferase (γ-GT) were measured by enzymatic tests (Hitachi Modular P800, Roche, Basel, Switzerland). Total cholesterol, HDL-cholesterol, LDL-cholesterol, and triacylglycerol concentrations (Roche) were calculated as previously described.[13] High sensitivity C-reactive protein (CRP) was measured using the Tinaquant CRP (Latex) ultrasensitive assay (Roche). Insulin was measured by an enzyme-amplified chemiluminescence assay (IMMULITE; Diagnostics Products Corp., Los Angeles, CA, USA). Intra- and inter-assay coefficients of variation were 4.2% and 5.7%, respectively. Insulin resistance and sensitivity were calculated using the homeostasis model assessment (HOMA) and a quantitative insulin sensitivity check index (QUICKI), respectively. Leptin was quantified by a double-antibody RIA method (Linco Research, Inc, St. Charles, MO, USA).[14,15] Intra- and inter-assay coefficients of variation were 6.7% and 7.8%, respectively. All reported investigations were carried out in accordance with the principles of the Declaration of Helsinki, as revised in 2013, and approved by the Hospital's Ethical Committee for Research (061/2014). Written informed consent was obtained from all participants.

2.2 | Adeno-associated vectors

AAV vectors, serotype 9, were used to drive the expression of GFP (AAV9-GFP) or hCPT1AM (AAV9-hCPT1AM) in mouse liver. Plasmid vectors carried: (a) the human albumin enhancer element and the human α1-antitrypsin (EalbAATp) liver-specific promoter described by Kramer et al,[16] (b) the cDNA sequence of GFP or hCPT1AM, (c) The woodchuck posttranscriptional regulatory element (WPRE, acc #AY468-486),[17] (d) The bovine growth hormone polyadenosine transcription termination signal [bGH-poly(A)] (bases 2326-2533 GenBank acc #M57764). The expression cassette was flanked by two-inverted terminal repeats (ITRs) derived from AAV2. The vector preparations used titers of 1.34×10^{13} and 1.16×10^{13} genome copies (gc)/mL for AAV9-GFP and AAV9-hCPT1AM, respectively.

2.3 | Animals

The animal study was designed as follows: 40 seven-week-old male C57BL/6J mice were purchased from Janvier (SC-C57J-M) and housed in our animal facility for 1 week to acclimatize. Mice were kept at standard laboratory conditions (12 hours light/dark cycle, 20-22ºC). Animals were randomly assigned to one of the following groups: NCD-GFP, HFD-GFP, NCD-hCPT1AM, and HFD-hCPT1AM. Five animals from each group were housed in the same cage. Next, mice were fed with either NCD (manufactured by TestDiet [catalogue number #58Y2], 10% kcal fat) of HFD

(manufactured by TestDiet [catalogue number #58Y1], 60% kcal fat) for the entire duration of the experiment. This diet causes steatosis but not severe liver injury (fibrosis). Body weight was measured every week and blood glucose once a month. After 9 weeks of diet, most of the mice already showed an obese phenotype characterized by a significant increase in circulating levels of glucose and insulin and higher body weight than the control NCD-fed group. AAV9-hCPT1AM and AAV9-GFP vectors were administered by tail-vein injection with a single dose (1.5×10^{12} gc/kg). To do that, mice were anesthetized in the morning (~10 AM) using isoflurane, and then, placed in a restrainer for the tail-vein injection. After injection, mice were returned to their home cage and room. Eleven weeks after virus injection, mice were anesthetized using isoflurane, and then, killed by cervical dislocation in fasting conditions (6 hours). The total duration of the HFD feeding paradigm was 20 weeks (9 weeks before AAV9 vector administration and 11 weeks after that). The Animal Experimentation Ethics Committee of the University of Barcelona (CEEA-UB) approved all the procedures with mice. Permits 9611 and 9609 were obtained from the Government of Catalonia, according to European Directive 2010/63/EU.

2.4 | Construction of site-directed hCPT1AM

hCPT1A wild-type (wt) cDNA (GenBank Access No. HGNC: 2328) was obtained by hCPT1A cDNA amplification from the HepG2 cell line. The primers used were: hCPT1AHindIII.for (5′TCGATAAGCTTATAAA ATGGCAGCTCACCAAGC3′) and hCPT1AEcoR1.rev (5′CATCCGGAATTCCTTTTTGGAATTAGA ACTG3′). The amplification was cloned in pYES plasmid to obtain the construct pYEShCPT1Awt. Plasmid pYEShCPTIAM593S was constructed using the Quick-Change PCR-based mutagenesis procedure (Stratagene) with the YEShCPT1Awt plasmid as template. Appropriate substitutions and the absence of unwanted mutations were confirmed by sequencing the inserts in both directions using Applied Biosystems 373 automated DNA sequences. To check hCPT1AM insensitivity to malonyl-CoA, we expressed the constructs containing hCPT1A wt and mutant (hCPT1AM) in yeast cells, and then, prepared cell extracts as described in Ref. (9) for the assay of CPT1 activity. *S cerevisiae* was chosen as an expression system for hCPT1A wt and hCPT1AM because it does not have endogenous CPT1 activity. The cDNA of the hCPT1AM gene used in our study contains the NH_2-terminal sequence that direct the protein to the mitochondria and two more sequences that codify for two α-helix fragments that insert this protein into the mitochondrial outer membrane.[18–20]

2.5 | Isolation of primary mouse hepatocytes

The collagenase method was used to isolate primary mouse hepatocytes.[21] Livers were perfused with Hank's balanced salt solution (HBSS, pH 7.4, 37°C, gassed with 95% O_2 and 5% CO_2: 5.4 mM KCl, 0.44 mM KH_2PO_4, 138 mM NaCl, 4.17 mM $NaHCO_3$, 0.338 mM Na_2HPO_4, 5.56 mM glucose, 50 mM HEPES, and 0.5 mM EGTA) through the portal vein for 5 minutes at a rate of 5 mL/min. Then, livers were perfused with HBSS (without EGTA) containing 5 mM of $CaCl_2$ and 0.25% (w/v) collagenase IV (Sigma) for 15 minutes approximately. The liver was then removed and gently teased apart in HBSS, and the cell suspension was washed three times in HBSS. Cell viability as assessed by the trypan blue exclusion test was always higher than 80%. Hepatocytes were seeded at a density of 3.5×10^6 cells in 0.1% (w/v) gelatin-treated 25-cm^2 flasks in DMEM medium (Gibco #11966), supplemented with 10% of FBS, 10 mM of glucose, 10 μg/mL of streptomycin, 100 units/mL of penicillin, 100 nM of dexamethasone (Sigma), and 100 nM of insulin (Sigma).

2.6 | Fatty acid oxidation

Fatty acid oxidation (FAO) to CO_2 and acid-soluble products (ASPs), essentially consisting of acyl-carnitine, Krebs-cycle intermediates, and acetyl-CoA, was measured in isolated primary mouse hepatocytes cultured in 25-cm^2 flasks. Following cell attachment after isolation (approximately 5 hours), the medium was replaced for 16 hours by fresh FAO medium (DMEM medium containing 0.1% FA-free BSA, 1 mM carnitine, 20 mM glucose, 10 nM insulin, 10 μg/mL streptomycin and 100 units/mL penicillin). Then, the medium was replaced by fresh FAO medium containing 0.3 mM of oleate and 1 μCi/ml [1-^{14}C]oleic acid bound to 1% (w/v) BSA and hepatocytes were incubated for 3 hours at 37°C in a CO_2-free incubator. Oxidation to CO_2 and ASPs was measured as described previously.[22]

2.7 | Isolation of mitochondria from liver and assay of CPT1 activity

Mitochondrial-enriched fractions from cultured hepatocytes were obtained by differential centrifugation. Briefly, hepatocytes were scraped and resuspended in 2 mL of solution A (70 mM sucrose, 220 mM mannitol, 2 mM EDTA, 5 mM HEPES, and protease inhibitor cocktail from Roche, pH 7.4). Then, cells were homogenized using a glass Wheaton-Dounce homogenizer (20 strokes with both the loose and the tight pestle) and centrifuged at 2000 *g* for 3 minutes at 4°C. Next, the supernatant was centrifuged at 16 000 *g* for 30 minutes at 4°C. Finally, the mitochondria-enriched pellet

was resuspended in 50-100 μL of solution A. CPT1 activity was measured in 10 μg of protein from those mitochondria-enriched fractions, using the radiometric method as described previously.[23] Concisely, the substrates L-[methyl-^{3}H]carnitine and palmitoyl-CoA were added to the protein suspension and enzyme activity was assayed for 4 minutes at 30°C in a total volume of 200 μL. Next, butanol was used to isolate the fraction containing the [^{3}H]palmitoyl-carnitine and radioactivity was measured by liquid scintillation counting.

2.8 | Serum biochemical analyses

Blood samples were obtained from the tails of awake mice after an overnight fast. Blood glucose concentrations were measured using a Glucometer Elite (Bayer). Serum insulin was measured by ELISA (Millipore). Plasma triacylglycerides, β-hydroxybutyrate, cholesterol, HDL cholesterol, AST, and ALT were determined enzymatically using commercial kits adapted to a COBAS 6000 autoanalyzer (Roche Diagnostics, Rotkreuz, Switzerland).[24]

2.9 | Glucose tolerance test

For the GTT, glucose (2.0 g per kg body weight) was dissolved in PBS and administered by intraperitoneal injection after an overnight fast. Then, blood glucose concentrations were measured using a Glucometer Elite (Bayer) before, 15, 30, 60, 90, and 120 minutes after administration.

2.10 | Analysis of insulin/AKT signaling pathway in hepatocytes

Analyses of insulin/AKT signaling were performed in isolated primary mouse hepatocytes. Sixteen hours after isolation, cells were incubated with 100 nM of insulin (Humulin 100 UI/mL, Lilly) for 5 minutes. After that, protein extracts from cells were used to measure phosphorylation of AKT using Western blot, as described below.

2.11 | Western blot

Protein determination by Western blot was performed using standard methods. CPT1A detection was undertaken in mitochondria-enriched fractions. The antibodies used are the following: Rabbit CPT1A-specific polyclonal antibody produced in our laboratory against amino acids 317-430 of the rat CPTIA,[10] Sci Crunch Cat# CPT1A, RRID:AB_2636894 (1:6000 in 5% Milk PBS-Tween); LC3B, Cell signaling #2775 (1:1000 in 5% Milk PBS-Tween); SQSTM/p62, Cell signaling #5114S (1:1000 in 5% Milk PBS-Tween); PLIN2, Abcam #Ab37516 (1:200 in 5% Milk PBS-Tween); PLIN5, Abcam #Ab192749 (1:2000 in 5% Milk PBS-Tween); LDLr, Abcam #Ab52818 (1:1500 in 5% Milk PBS-Tween); LRP1, Abcam #Ab92544 (1:7000 in 5% Milk PBS-Tween); VLDLr, Santa Cruz #sc-18824 (1:1500 in 5% Milk PBS-Tween); TIM44, BD Bioscience #612582 (1:5000 in 5% Milk PBS-Tween); pAkt (Ser473), Cell signaling #4051S (1:1000 in 5% Milk PBS-Tween); Akt, Cell signaling #9272S (1:1000 in 5% Milk PBS-Tween); UCP2, Cell signaling #89326 (1:1000 in 5% Milk PBS-Tween); HMGS2, produced in our laboratory (1:6000 in 5% Milk PBS-Tween); β-actin, Sigma Aldrich #A3854 (1:50.000 in PBS-Tween); Total OXPHOS Rodent WB Antibody Cocktail, Abcam #ab110413 (1:5000 in 5% Milk PBS-Tween); Lipolysis Activation Antibody Sampler Kit, Cell signaling #8334 (for all antibodies 1:1000 in 5% Milk PBS-Tween); ATGL, Cell signaling #2138 (1:1000 in 5% Milk PBS-Tween).

2.12 | Measurements of liver TAG content

To measure TAG content in the liver, 100 mg of frozen tissue were homogenized in 500 μL of PBS. Then, chloroform-extracted lipids were dried under an N_2 stream and dissolved in isopropanol. TAG were quantified in the extracted lipids using the Cromatest Triglycerides MR kit (Linear Chemicals SL).

2.13 | ATP extraction and measurement

Frozen liver samples were powdered and homogenized in 1.0 mL of 40% ice-cold HCLO4 and incubated for 10 minutes. The precipitated proteins were removed by centrifugation (10 000 *g* for 10 minutes). Next, 300 μL of the supernatant was neutralized by 5 M KHCO3. Then, 10 μL was pipetted into the wells of a white nonphosphorescent microplate, placed in a luminometer (Turner System), and processed by addition of 90 μL of ATP monitoring reagent (Molecular Probe, Life Technologies A22066). ATP concentrations were calculated from a calibration curve constructed at the same time by means of standard ATP dissolved in the appropriate solution for each experiment.

2.14 | Measurement of oxygen consumption in isolated mitochondria

Respiration of isolated liver mitochondria (500 μg protein) was measured at 37°C by high-resolution respirometry with the Oxygraph-2k (OROBOROS INSTRUMENTS, Innsbruck, Austria). Mitochondria were obtained in buffer

II (sucrose 0.5 M, KCl 50 mM, EDTA 5 mM, sodium pyrophosphate 1 mM, $MgCl_2$ 5 mM, pH 7.4, and protease inhibitors) and 500 µL of mitochondria was brought to a final volume of 2.1 mL with respiration medium (EGTA 0.5 mM, $MgCl_2.6H_2O$ 3 mM, taurine 20 mM, KH_2P0_4 10 mM, HEPES 20 mM, BSA 1 g/l, K-lactobionate 60 mM, sucrose 110 mM, pH 7.1) and added into the oxygraph chamber. All respiration measurements were made in triplicate. Resting respiration (state 4, absence of adenylates) was assessed by the addition of 10 mM glutamate and 2 mM malate as the complex I substrate supply. Then, state 3 respiration was assessed by the addition of 2.5 mM ADP. RCR was calculated as the quotient state 3/state 4. The integrity of the outer mitochondrial membrane was established by the addition of 10 µM cytochrome c and no stimulation of respiration was observed. The addition of 10 mM succinate provided state 3 respiration with parallel electron input to complexes I and II. The concentrations of substrates and inhibitors used were based on prior experiments conducted for optimization of the titration protocols.

2.15 | Measurements of liver temperature

The thermal images from mice liver were made using a FLIR T420 infrared camera (FLIR T420 Systems AB, Sweden) with thermal sensitivity of 0.05°C and resolution set at 320 × 240 pixels. Mice were anesthetized and their abdominal cavity was opened. The first image was taken of a piece of aluminum foil to obtain a measurement of the reflected temperature for each set of images. To take the images, the camera was placed 30 cm from the midpoint of the liver. Thermal data were extracted from the pictures using a region of interest (ROI)-based approach. The ROIs were manually drawn in the images of the liver region using FLIR Research IR Max software version 4.40.6.24 for Windows (FLIR Systems Inc, North Billerica, MA, USA). The reflected temperature was obtained by placing a rounded ROI on the aluminum foil image and retaining the mean value (°C) for adjustments. Images were not normalized by liver size or weight, since the thermographic camera measures the minimum and maximal temperatures for a given ROI. Thus, these measurements do not vary according to liver size or weight.[25]

2.16 | RNA extraction and quantitative RT-PCR

RNA extraction and quantitative RT-PCR were performed using standard procedures. Briefly, total RNA was extracted from frozen, pulverized tissue using the RNeasy kit (QIAGEN). Then, cDNA was synthesized with the Transcriptor First Strand cDNA Synthesis kit (Roche). For PCR amplifications, the LightCycler 480 SYBR Green I Master kit (Roche) was used and measured with the Roche LightCycler 480 Real-Time PCR System. The sequences of the oligonucleotides used are:

Abca1 For: 5′-TTCTTGCGATACACTCTGGTGC Rev: 5′-CGGGATTGAATGTTCTTGTCGT;
Atgl For: 5′-TGACCATCTGCCTTCCAGA Rev: 5′-TGTGGTGGCGCAAGAACA;
Atg7 For: 5′-CCGGTGGCTTCCTACTGTTA Rev: 5′-AAGGCAGCGTTGATGACC;
β-actin For: 5′-ATGCTCCCCGGGCTGTAT Rev: 5′-CATGGAGTCCTTCTGACCCAT;
Hsl For: 5′-GCGCTGGAGGAGTGTTTTT Rev: 5′-CGCTCTCCAGTTGAACCAAG;
Mgl For: 5′-TGAGAAAGGCTTTAAGAACTGGG Rev: 5′-GACCACCTGTGTGATGTGGG;
Mtp For: 5′-GTGGAGGAATCCTGATGGTGA Rev: 5′-TGATCTTGGTGTACTTTTGCCC;
hcpt1a For: 5′-CAATCGGACTCTGGAAACG Rev: 5′-CCGCTGACCACGTTCTTC.

For *Abcg8c* and *Abcg5* gene expression analyses, cDNA was subjected to real-time PCR amplification using TaqMan Master Mix (Applied Biosystems) and specific mouse TaqMan probes (Applied Biosystems) (Mm00446241_m1 [Abcg5] and Mm00445970_m1 [Abcg8]).

2.17 | Oil Red O staining in hepatocytes

TAG content in isolated primary mouse hepatocytes was measured using Oil Red O staining (Sigma, O0625), following standard procedures. Oil Red O stock solution was prepared in isopropanol (3 mg/mL). It was then filtered after overnight agitation and stored protected from light. The Oil Red O working solution was prepared by diluting the stock 3:2 in distilled water. Sixteen hours after hepatocyte isolation, cells were washed twice with PBS and fixed using formalin 4% of formaldehyde for 30 minutes at room temperature. After fixation, hepatocytes were washed again with PBS, and then, permeabilized for 30 minutes with 60% of isopropanol. Next, cells were incubated with Oil Red O working solution for 15 minutes. Finally, cells were washed with water and examined under the microscope. Lipid-packed vesicles appear as bright red after Oil Red O staining.

2.18 | Autophagy flux assay

Autophagy/LC3II flux was performed in isolated primary mouse hepatocytes. Sixteen hours after isolation cells were incubated with chloroquine (CQ) (20 µM) for 6 hours. After that,

protein extracts from cells were used to measure LC3II protein levels using western blot, as described above. Autophagy flux was calculated by subtracting the densitometry values of LC3II in CQ untreated from CQ-treated samples.

2.19 | Determination of acylcarnitine content

To determine the acylcarnitines in liver and serum samples, 140 μL of serum and tissue homogenate was used for acylcarnitine extraction. First, 10 μL of Deuterated palmitoylcarnitine [20 μM] was added to get 200 pmol in 150 μL of final resuspension. Next, 750 μL of Folch reagent (chloroform:metanol 2:1), 100 μL of dH_2O and 50 μL 0.1 M KOH were added to the samples. Phases were separated after vortexing and centrifugation at 2000 rcf. Following, the top aqueous phase was carefully removed and the organic phase containing the acylcarnitines was washed with 200 μL of methanol:dH_2O:chloroform (48:47:3). After washing, the organic solvent was dried using a SpeedVac vacuum concentrator. The day of the analyses, samples were resuspended with 150 μL of methanol. Acylcarnitines were analyzed using an Acquity UPLC-TOF system (Waters) with an BEH C8 column (1.7 mm particle size, 100 mm, 62.1 mm, Waters). The two mobile phases were 1 mM of ammonium formate in methanol (phase A) and 2 mM of ammonium formate in H2O (phase B), both phases with 0.05 mM of formic acid. The following gradient was programed: 0 minute, 65% A; 10 minutes, 90% A; 15 minutes, 99% A; 17 minutes, 99% A; 20 minutes, 65% A, and a flow rate of 0.3 mL min^{-1}. Quantification was carried out using the extracted ion chromatogram of each compound, using 50-mDa windows. The linear dynamic range was determined by injecting standard mixtures. Positive identification of compounds was based on the accurate mass measurement with an error, 5 ppm and their LC retention time compared to that of a standard (62%).

2.20 | Lipidomic analyses

2.20.1 | Phospholipids and neutral lipids

A total of 750 μL of a methanol-chloroform (1:2, vol/vol) solution containing internal standards (16:0 D31_18:1 phosphocholine, 16:0 D31_18:1 phosphoethanolamine, 16:0 D31-18:1 phosphoserine, 17:0 lyso-phosphocholine, 17:1 lyso-phosphoethanolamine, 17:1 lyso-phosphoserine, 17:0 D5_17:0 diacylglycerol, 17:0/17:0/17:0 triacylglycerol and C17:0 cholesteryl ester, 0.2 nmol each, from Avanti Polar Lipids) were added to 0.020 mL of serum. Samples were vortexed and sonicated until they appeared dispersed. They were extracted at 48°C overnight. The samples were then evaporated and transferred to 1.5 mL Eppendorf tubes after the addition of 0.5 mL of methanol. Samples were evaporated again and resuspended in 150 μL of methanol. The tubes were centrifuged at 13 000 *g* for 3 minutes, and 130 μL of the supernatants was transferred to ultra-performance liquid chromatography (UPLC) vials for injection and analysis.

2.20.2 | Sphingolipids

A total of 750 μL of a methanol-chloroform (2:1, vol/vol) solution containing internal standards (N-dodecanoylsphingosine, N-dodecanoylglucosylsphingosine, N-dodecanoylsphingosylphosphorylcholine, and C17-sphinganine, 0.2 nmol each, from Avanti Polar Lipids) were added to 0.05 mL of serum. Samples were extracted at 48°C overnight and cooled. Then, 75 μL of 1 M KOH in methanol was added, and the mixture was incubated for 2 hours at 37°C. Following addition of 75 μL of 1 M acetic acid, samples were evaporated to dryness, and stored at −20°C until analysis. Before analysis, 150 μL of methanol were add to the samples, centrifuged at 13 000 *g* for 5 minutes and 130 μL of the supernatant were transferred to a new vial and injected.

LC-HRMS analysis was performed using an Acquity ultra high-performance liquid chromatography (UHPLC) system (Waters, USA) connected to a Time of Flight (LCT Premier XE) Detector. Full scan spectra from 50 to 1800 Da were acquired, and individual spectra were summed to produce data points each of 0.2 seconds. Mass accuracy at a resolving power of 10 000 and reproducibility were maintained using an independent reference spray via the LockSpray interference. Lipid extracts were injected onto an Acquity UHPLC BEH C8 column (1.7 μm particle size, 100 mm × 2.1 mm, Waters, Ireland) at a flow rate of 0.3 mL/min and a column temperature of 30°C. The mobile phases were methanol with 2 mM of ammonium formate and 0.2% of formic acid (A)/water with 2 mM of ammonium formate and 0.2% of formic acid (B). A linear gradient was programed as follows: 0.0 minutes: 20% B; 3 minutes: 10% B; 6 minutes: 10% B; 15 minutes: 1% B; 18 minutes: 1% B; 20 minutes: 20% B; 22 minutes: 20% B.

Sphingolipids (Cer, ceramide; SM, sphingomyelin; GlucCer, glucosylceramide; HexCer: hexosylceramides), glycerophospholipids (PC, phosphatidylcholine; LPC: lysophosphatidylcholine; pPC: plasmanylcholine; LPEA: lysophosphatidylethanolamine; and PC O-: ether-linked phosphatidylcholine), neutral lipids (DAG: diacylglycerol; TAG: triacylglycerol; CE: cholesterol ester). All Lipid species are annotated using the "lipid subclass" and "C followed by the total fatty acyl chain length:total number of unsaturated bonds" and (eg, PC (C32:2)).

2.21 | Statistical analysis

Data are presented as mean ± SEM. For the statistical analyses, we used analyses of variance considering two factors

(two-way ANOVA: factor one was diet [NCD or HFD] and factor two was the virus injected [AAV-GFP or AAV-hCPT1AM]), followed by Tukey's multiple comparison test. For the lipidomic studies of mice samples, we used two-way ANOVA analysis, correcting for multiple comparisons by controlling the false discovery rate (FDR) (two-stage step-up method of Benjamini, Kieger, and Yekutieli). Hierarchical clustering was performed using R.[26] For these analyses, preprocessed lipidomics data were log-transformed and normalized between samples using limma package.[27] To avoid mathematical errors, before log-transformation zeros were substituted by 1/10th of the minimum value (other than zero) in the data matrices. Hierarchical unsupervised clustering was performed using heatmap 3 package,[28] applying complete linkage on the euclidean distances matrices. For the analysis of human lipidomic measurements, principal component analyses (PCA) were performed using the function prcomp from R base after scaling the log-transformed data to account for the large numerical differences among the mean values of the different lipidic molecules. UMAP analyses were performed on log-transformed data using R umap package[29] that implements the Uniform Manifold Approximation and Projection method.[30] The lipid content change (ΔLC) was calculated for every lipid in obese patients as the difference in the log-transformed content of that particular lipid after surgery vs before surgery. Similarly, changes in NAFLD-related parameters were calculated in obese patients as the difference in those parameters after surgery. Partial correlations between ΔLC and changes in NAFLD-related, correcting for age, gender, and changes in BMI were calculated using the package ppcor[31] and visualized using corrplot package.[32] Essentially, the partial correlation analyses evaluated the lineal regression equation "ΔNAFLD.variable ~age +gender + ΔBMI + Δlipid.content," where ΔNAFLD.variable was the change in the studied variable (ie, glucose, AST, ALT, GGT, or ADT/ALT) after surgery, ΔBMI was the change in BMI after surgery and Δlipid.content was the change of the studied lipid after surgery. When required, *P* values were adjusted for multiple testing using the false discovery method (FDR)[33] implemented in the function p.adjust. When very strong correlation among tests was expected (for instance, in the partial correlation analyses), no further *P* value adjustment was applied to minimize type-II errors. Differences were considered significant at $P < .05$.

3 | RESULTS

3.1 | AAV9-mediated expression of hCPT1AM in mouse liver increases FAO

We used AAVs to express a human mutated isoform of CPT1A (hCPT1AM) or green fluorescent protein (GFP), which was used as a control (AAV9-hCPT1AM and AAV9-GFP, respectively). The genome of each virus contained the target gene under the control of the liver-specific promoter EalbAATp, which constrained the expression of hCPT1AM to this tissue (Figure S1A).

Eight-week old C57Bl/6J mice were fed either NCD or HFD for 9 weeks. After that time, mice showed an obese phenotype characterized by a significant increase in circulating levels of glucose and insulin and higher body weight than the control NCD-fed group (Figure S1B-C). NCD- and HFD-fed mice were then administered 1.5×10^{12} gc/kg of AAV9-GFP or AAV9-hCPT1AM by tail-vein injection (Figure 1A). Mice were studied throughout the treatment and killed at 11 weeks after AAV administration. At that time point, most hepatocytes expressed GFP in both NCD- or HFD-fed mice treated with AAV9-GFP, which indicated that the infection efficiency was similar in both groups (Figure S2A). As expected, mRNA expression of hCPT1A was observed in NCD-hCPT1AM and HFD-hCPT1AM mice but not in their respective GFP controls (Figure S2B). In addition, CPT1A protein levels were 2- and 1.7-fold higher in NCD-hCPT1AM and HFD-hCPT1AM mice, respectively, than in their GFP controls (Figure S2C). Note that the CPT1A antibody recognizes both endogenous CPT1A and the expressed hCPT1AM protein. Concomitantly, CPT1 activity was 1.62-fold higher in NCD-hCPT1AM mice and 1.42-fold higher in HFD-hCPT1AM mice than in their respective GFP controls (Figure 1B). To discard changes in mitochondrial content due to hCPT1AM expression, we analyzed mitochondrial protein TIM44 (translocase of the mitochondrial inner membrane) levels in the liver of all mice. No differences were seen in mitochondrial content between groups (Figure S2D). CPT1A protein levels in other tissues with strong AAV9 tropism, such as heart and skeletal muscle (hamstring), did not change after administration of AAV9-hCPT1AM (Figure S2E).

Consistent with increased CPT1 protein and activity, the levels of long-chain acylcarnitines, which are direct products of CPT1A activity, were increased in the liver of hCPT1AM-expressing mice compared to GFP-expressing controls (Figure 1C). Conversely, long-chain acylcarnitine concentrations in serum samples were similar among all groups (Figure 1C). Moreover, FAO was 32% higher in cultured primary hepatocytes from HFD-hCPT1AM mice than in HFD-GFP controls (Figure 1D). The same was true in hepatocytes from NCD-hCPT1AM mice, albeit to a lesser extent.

3.2 | hCPT1AM expression in mouse liver reduces hepatic steatosis, hepatic insulin resistance, hyperglycemia, and hyperinsulinemia

HFD-hCPT1AM mice weighed significantly less than HFD-GFP control mice, whereas no differences were seen

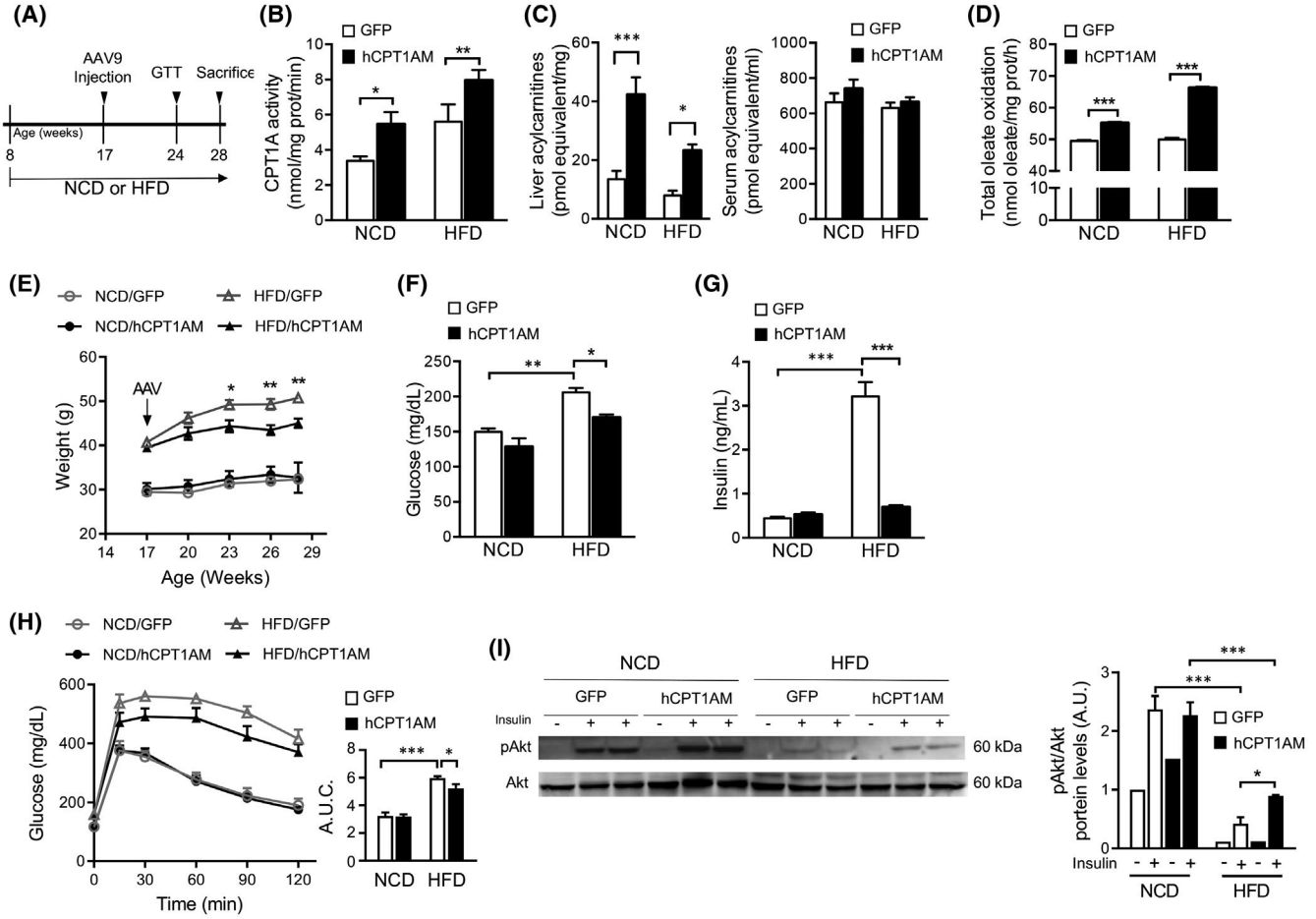

FIGURE 1 Expression of hCPT1AM increases FAO in hepatocytes and improves metabolic parameters and decreases hepatic steatosis in HFD-fed obese mice. A, Experiment design and time course. B, CPT1A activity in isolated mitochondria from NCD- and HFD-fed mice expressing either GFP or hCPT1AM. C, Long-chain acylcarnitines were measured in liver and serum samples from GFP- and hCPT1AM-expressing mice as an indirect indicator of CPT1A activity. D, Total oleate oxidation in isolated hepatocytes from NCD- and HFD-fed mice expressing either GFP or hCPT1AM. E, Body weight (*$P < .05$, **$P < .01$, HFD-GFP vs HFD-hCPT1AM) of NCD- and HFD-fed mice after treatment with AAV9-GFP or AAV9-hCPT1AM. Fasting blood (F) glucose and (G) insulin levels NCD- and HFD-fed mice after treatment with AAV9-GFP or AAV9-hCPT1AM. H, Glucose tolerance test of NCD- and HFD-fed mice after treatment with AAV9-GFP or AAV9-hCPT1AM. I, Insulin signaling in isolated hepatocytes from NCD- and HFD-fed mice expressing either GFP or hCPT1AM, as indicated by Western blotting of insulin-induced Akt phosphorylation (pAkt, Ser473). Quantification of pAkt normalized by total Akt (N = 4). AU =arbitrary units. N = 5-6 (unless stated otherwise), *$P < .05$, **$P < .01$, ***$P < .001$

in NCD-hCPT1AM mice (Figure 1E and Table 1). The differences in body weight were not attributable to changes in food consumption, since daily rates of food intake were equal in GFP- and hCPT1AM-expressing mice fed either NCD or HFD (Figure S3A). Fasting blood glucose and insulin levels were lower in HFD-hCPT1AM mice than in control HFD-GFP mice, and similar to levels observed in NCD-treated mice (Figure 1F-G). Glucose tolerance (measured via intraperitoneal GTT) was improved in HFD-hCPT1AM mice compared to HFD-GFP control mice (Figure 1H). In addition, pAkt levels were higher in cultured primary hepatocytes from HFD-hCPT1AM mice than in those from HFD-GFP mice, as shown in Figure 1I. Overall, these results indicate that hCPT1AM expression improves hepatic insulin signaling and the obesity-induced diabetic phenotype observed in HFD-fed mice.

Liver weight and TAG content of HFD-hCPT1AM mice were lower than in HFD-GFP control mice (Figure 2A, Table 1 and Figure S3B). In addition, histopathological analysis of liver samples confirmed that HFD-hCPT1AM mice showed a reduction in the NAFLD activity score (NAS)[34] (Table S1). Furthermore, hepatocellular ballooning was not observed in any of the HFD-hCPT1AM mice (Table S1). Of note, hCPT1AM expression did not significantly affect liver histological parameters in NCD-fed mice (Figure 2A and Table S1). Finally, hepatic injury was lower in HFD-hCPT1AM mice than in HFD-GFP controls, as indicated by lower serum levels of AST and ALT enzymes (Table 1). In

TABLE 1 Analyses of body weight, serum enzymes and metabolites, liver weight and liver triglyceride (TAG) content in mice

	NCD		HFD	
	AAV-GFP	**AAV-hCPT1AM**	**AAV-GFP**	**AAV-hCPT1AM**
Body weight (g)	32.3 ± 0.86	32.7 ± 1.41	50.7 ± 0.99#	45 ± 1.02*
Total CHOL (mg/dL)	105.0 ± 7.58	107.8 ± 9.06	205.2 ± 6.52#	180.2 ± 7.36*
TAG (mg/dL)	39.8 ± 2.97	42.2 ± 7.14	42.8 ± 1.35	38.8 ± 1.74
LDL CHOL (mg/dL)	29.8 ± 4.68	33.7 ± 4.32	117.2 ± 6.44#	89.3 ± 6.28*
HDL CHOL (md/dL)	67.1 ± 2.91	65.6 ± 4.55	79.4 ± 0.96	82.6 ± 1.69
BHB (mM)	1.2 ± 0.06	1.1 ± 0.08	1.5 ± 0.09#	1.9 ± 0.10*
ALT (U/L)	8.3 ± 1.66	4.2 ± 1.72	109.2 ± 22.50#	34 ± 5.75*
AST (U/L)	35.2 ± 5.31	27.3 ± 2.22	110.4 ± 18.33#	67.2 ± 8.41*
Liver weight (g)	1.1 ± 0.04	1.1 ± 0.08	2.4 ± 0.12#	1.5 ± 0.10*
Liver TAG (mg/g liver)	2.2 ± 0.12	1.2 ± 0.06	48 ± 0.67#	29.4 ± 0.50*

Note: Measures were performed in 28-week old mice, 11 weeks after injection of the AAV9s. Data are means ± SEM. n = 5-6.

Abbreviations: ALT, alanine aminotransferase; AST, aspartate aminotransferase; BHB, β-hydroxybutyric acid; CHOL, total cholesterol; HDL, high-density lipoprotein cholesterol; HFD, high-fat diet; LDL, low-density lipoprotein cholesterol; NCD, normal chow diet.

*$P < .05$ versus HFD-GFP;

#$P < .01$ versus NCD-GFP.

summary, these results indicate that hepatic hCPT1AM expression decreases HFD-induced hepatic steatosis and injury.

3.3 | Increased liver FAO activates mitochondrial energy metabolism

Increased FAO due to hCPT1AM expression could produce a surplus of acetyl-CoA that can be metabolized by two pathways: (1) conversion to ketone bodies and (2) entry to the tricarboxylic acid (TCA) cycle to complete oxidation. Oxidation of acetyl-CoA can be coupled to ATP synthesis or not, in which case uncoupling protein 2 (UCP2) allows the dissipation of energy as heat. First, we analyzed liver protein levels of mitochondrial hydroxymethylglutaryl-CoA synthase 2 (HMGCS2), the rate-limiting enzyme of hepatic ketogenesis. HMGCS2 protein levels were higher in hCPT1AM-expressing mice than in GFP control mice in both NCD- and HFD-fed groups (Figure 2B). In addition, serum levels of ketone bodies such as β-hydroxybutyric acid (BHB) were higher in HFD-hCPT1AM mice than in HFD-GFP control mice (Table 1). These results suggest that excess substrates in HFD-hCPT1AM mice promote the production of ketone bodies. Second, we observed that temperature and UCP2 protein levels were higher in the liver of HFD-hCPT1AM mice than in the HFD-GFP control group, which indicates an increase in energy dissipation (Figure 2B-C). Finally, liver ATP levels were higher in HFD-hCPT1AM mice than in control HFD-GFP mice (Figure 2D), whereas no differences were observed in NCD-fed mice. Altogether, these results indicate that hCPT1AM expression increments FAO in liver, resulting in an increase in ketogenesis and oxidative phosphorylation, both uncoupled and coupled to ATP synthesis.

Moreover, HFD reduced the mitochondrial respiratory control ratio (RCR) in GFP-expressing mice but not in hCPT1AM-expressing mice. This indicates higher respiratory coupling efficiency in liver mitochondria from HFD-fed hCPT1AM-expressing mice (Figures 2E and S3C). The protein levels of the OXPHOS complexes CV-ATP5A, CIV-MTCO1, CII-SDHB, and CI-NDUFB8 were similar in HFD-hCPT1AM and HFD-GFP control mice (Figure S3D). No alteration in the mRNA levels of the genes involved in mitochondrial dynamics was observed in any of the experimental groups (Figure S4A).

3.4 | hCPT1AM expression activates autophagy in liver

Because the expression of hCPT1AM in the liver of HFD-fed mice decreases the accumulation of lipid droplets (LD) (Table 1, Figures 2A and S3B), we next examined the two main catabolic pathways of LDs: lipolysis and autophagy. First, we measured the levels of perilipin 2 and 5 (PLIN2 and PLIN5), which are key components of the LDs and considered regulators of lipolysis.[35] HFD-induced increase in PLIN2 and PLIN5 protein levels was blunted in hCPT1AM-expressing mice (Figure 3A). Next, we analyzed the mRNA levels of the genes *Atgl*, *Hsl,* and *Mgl*, which encode enzymes involved in the lipolysis pathway. In all cases, values were higher in HFD-hCPT1AM than in HFD-GFP control mice (Figure S4B). However, no changes were observed when we analyzed the protein concentrations of the lipases ATGL

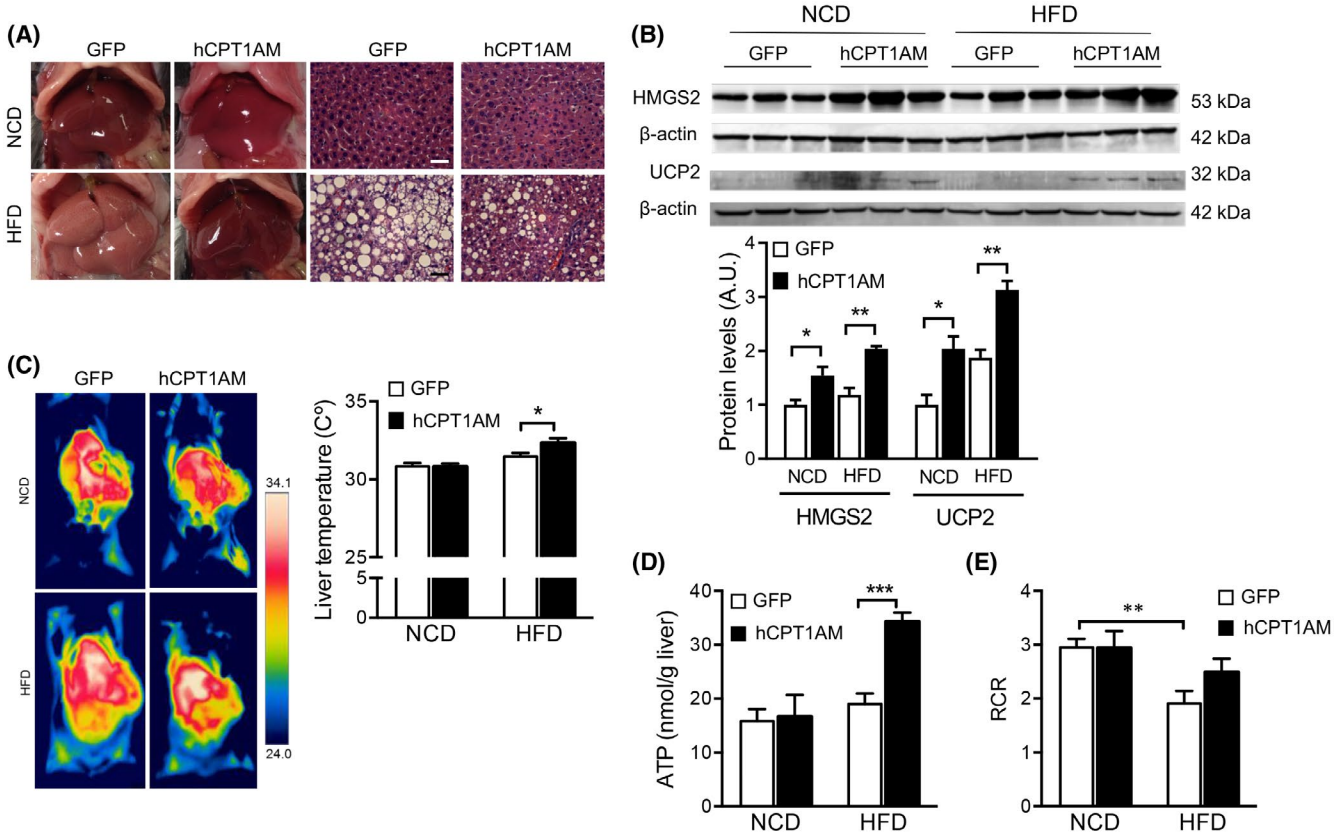

FIGURE 2 Expression of hCPT1AM decreases hepatic steatosis in HFD-fed obese mice. A, Liver macroscopic appearance (left panel), and histology (hematoxylin and eosin staining, scale bar is 50 μm) (right panel) in NCD- and HFD-fed mice after treatment with AAV9-GFP or AAV9-hCPT1AM. B, Protein levels of HMGCS2, the rate-limiting enzyme of hepatic ketogenesis, and UCP2 in liver of NCD- and HFD-fed mice expressing either GFP or hCPT1AM, as indicated by Western blotting. Quantification is normalized by β-actin (N = 3). C, Liver temperature as indicated by infrared thermography and D, liver ATP levels in NCD- and HFD-fed mice after treatment with AAV9-GFP or AAV9-hCPT1AM. E, Mitochondrial respiratory capacity in isolated mitochondria from NCD- and HFD-fed mice expressing either GFP or hCPT1AM. AU =arbitrary units. N = 5-6 (unless stated otherwise), $*P < .05$, $**P < .01$, $***P < .001$

and the phosphorylated active form of HSL (Figure S4C). Altogether, these results suggest that the decrease in LD observed in HFD-hCPT1AM mice is independent of the LD-associated lipases activity.

Recent studies have revealed a role for autophagy in LD breakdown.[36,37] Therefore, next we analyzed the expression of autophagy-related protein 7 (Atg7) and the protein levels of the LC3II/LC3I ratio and p62, autophagy biomarkers. ATG7 is a key protein in LC3II formation during the initial steps of the autophagy process. We observed that Atg7 mRNA levels were higher in HFD-hCPT1AM than in HFD-GFP control mice, which indicates an increase in the machinery to activate autophagy (Figure 3B). Moreover, the LC3II/LC3I ratio was higher and p62 protein levels were lower in HFD-hCPT1AM mice than in the HFD-GFP group (Figure 3C). Accumulation of LC3II in the presence of Chloroquine (CQ) indicates its flux through lysosomes. Of note, quantification of LC3II flux revealed an induction of autophagy in cultured hepatocytes from hCPT1AM-expressing mice when compared to GFP controls (Figure 3D). Altogether, these results suggest that hCPT1AM expression in HFD-fed mice increases the expression of the machinery of autophagosome formation.

3.5 | hCPT1AM expression improves cholesterol levels in HFD-fed mice

HFD-hCPT1AM mice showed considerably lower total and LDL-cholesterol in serum than obese HFD-GFP control mice (Table 1). To determine which mechanisms might be involved in the observed low serum cholesterol levels we analyzed: (1) mRNA levels for the key enzyme HMG-CoA reductase and the transcription factor SREBP-2 (both involved in de novo cholesterol synthesis), (2) protein levels of liver lipoprotein receptors, and (3) mRNA levels for transporters involved in liver cholesterol export. Our results showed no changes in HMG-CoA reductase and SREBP-2 mRNA levels due to hCPT1AM expression (Figure S4D). We next measured protein levels of liver lipoprotein receptors involved in the import and export of liver cholesterol. Specifically, we analyzed LDLr (low-density lipoprotein receptor), VLDLr (very-low-density lipoprotein

receptor), and LRP1 (low-density lipoprotein receptor-related protein). HFD-induced increase in LDLr protein levels was blunted in hCPT1AM-expressing mice (Figure 3E). No significant changes were observed in VLDLr and LRP1 protein levels. The mRNA levels for MTP (microsomal transporter protein), a protein involved in ApoB formation, were lower in HFD-GFP than in NCD-GFP mice and did not change after the expression of hCPT1AM (Figure 3F). The mRNA levels for ABCA1 and ABCG5/G8 transporters, which are involved in cholesterol export, were lower in obese HFD-GFP mice. However, hCPT1AM expression was sufficient to revert the decrease caused by HFD (Figure 3F). Altogether, these results suggest

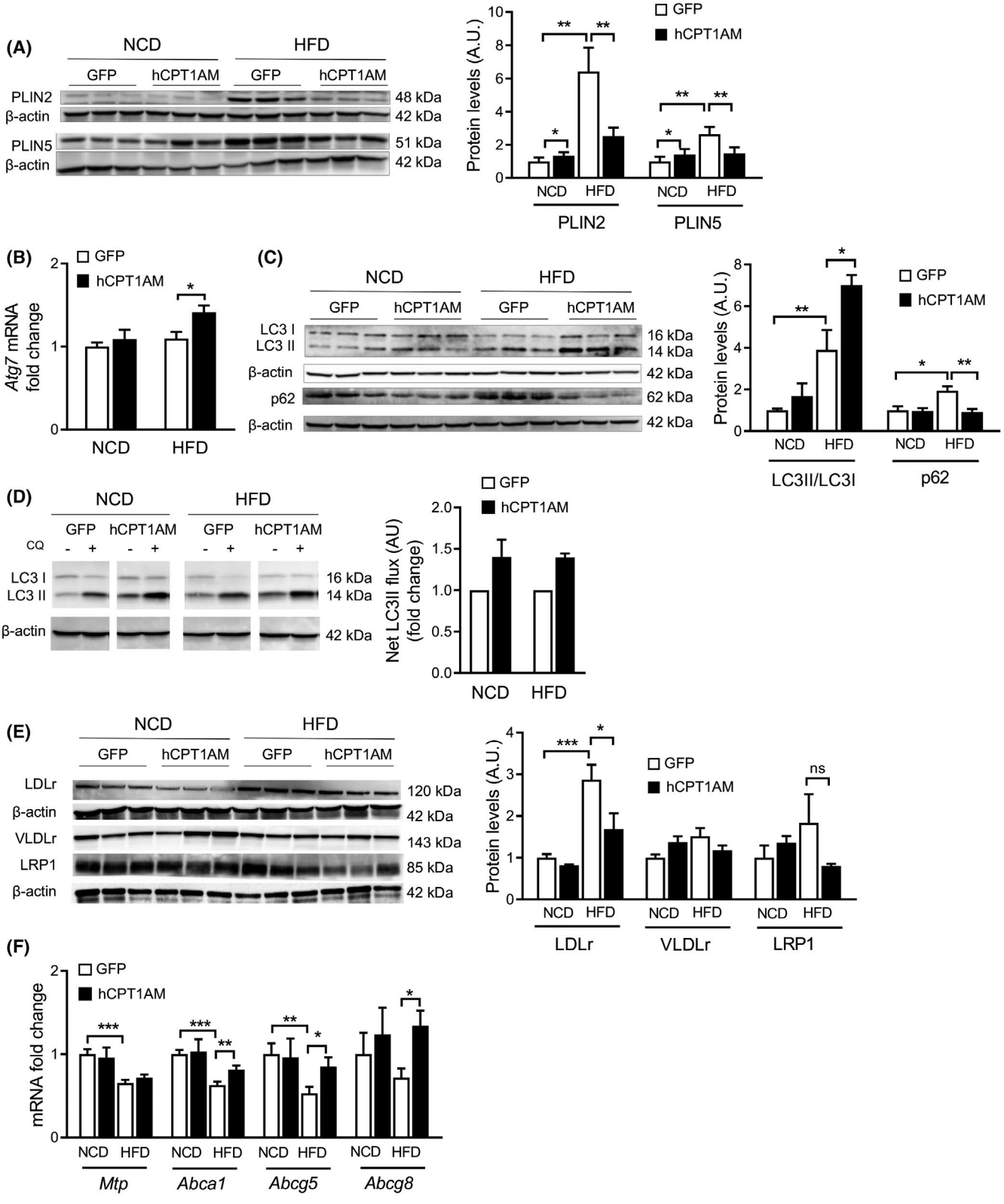

FIGURE 3 Expression of hCPT1AM in liver increases hepatic autophagy and modulates cholesterol metabolism in HFD-fed mice. A, Levels of PLIN2 and PLIN5 in liver of NCD- and HFD-fed mice expressing either GFP or hCPT1AM, as indicated by Western blotting. Quantification is normalized by β-actin. B, mRNA levels of *Atg7* in the liver of NCD- and HFD-fed mice after treatment with AAV9-GFP or AAV9-hCPT1AM. C, Levels of LC3I/II and p62 in the liver of NCD- and HFD-fed mice expressing either GFP or hCPT1AM, as indicated by Western blotting. Quantification is normalized by β-actin. (N = 3). D, Quantification of net autophagy flux in isolated hepatocytes from NCD- and HFD-fed mice expressing either GFP or hCPT1AM, as indicated by Western blotting of CQ-induced LC3II accumulation. Quantification is normalized by β-actin (N = 2). E, Levels of LDLr, VLDLr, and LRP1 in the liver of NCD- and HFD-fed mice expressing either GFP or hCPT1AM, as indicated by Western blotting. Quantification is normalized by β-actin (N = 3). F, mRNA levels of *Mtp, Abca1, Abcg5,* and *Abcg8* in the liver of NCD- and HFD-fed mice after treatment with AAV9-GFP or AAV9-hCPT1AM. AU =arbitrary units. CQ = chloroquine. N = 5-6 (unless stated otherwise), $^{*}P < .05$, $^{**}P < .01$, $^{**}P < .001$

that some aspects of liver cholesterol metabolism are improved in HFD-hCPT1AM mice, which could explain the reduction in total serum cholesterol levels observed in these mice.

3.6 | Comparative liver and serum lipidomic analysis of AAV9-hCPT1AM-treated mice shows a specific lipidomic signature to monitor hepatic steatosis

Reliable noninvasive methods to monitor NAFLD remain limited. Here, we aimed to uncover serum lipid biomarkers for noninvasive clinical detection and monitoring of hepatic steatosis. We performed a comparative lipidomic study in liver and serum samples from NCD- and HFD-fed mice expressing either GFP or hCPT1AM. We analyzed 66 species of sphingolipids, 16 species of glycerophospholipids, and 94 species of neutral lipids by electrospray ionization mass spectrometry (ESI-MS). In the liver, a subset of 42 lipids exhibited statistically significant differences among NCD-GFP and HFD-GFP groups (two-way ANOVA $P < .01$ adjusted for multiple comparisons using FDR) (Figure 4A). Noteworthy, expression of hCPT1AM in HFD-fed mice restored the levels of 30 of these lipid species to what is seen in NCD-fed mice (shown in red in Figure 4A). These include ceramides (Cer (C16:0, C18:0, C20:0, and C22:0)), dihydroceramides (dhCre (C22:0)) and phospholipids, specifically lysophosphatidylcholines (LPC (C16:0 and C18:0)). However, the most significant changes were observed in the levels of neutral lipids, such as DAG and TAG. While the livers of HFD-GFP mice show a vast increase in the levels of DAG and TAG, specifically those with a long-chain fatty acyl group, the expression of hCPT1AM in HFD-fed mice was sufficient to reverse the accumulation of these lipid species (Figure 4A). The clustering analysis was performed using complete linkage method on the euclidean distances of the log-transformed values of the 42 liver lipid biomarkers that showed statistically significant differences based on the type of diet. Accordingly, the classification provided by the clustering analysis mainly reflected the difference in diet, albeit it also clearly showed differences between the HFD-fed animals expressing hCPT1AM (all of them in the cluster in red) vs those expressing the control GFP protein (all but one in the cluster in green) (Figure 4A). As expected, not all the lipid species that changed in the liver of HFD-hCPT1AM mice were also changed in serum. As shown in Figure 4B, a subset of 24 lipids exhibited statistically significant differences between HFD-fed and NCD-fed mice (two-way ANOVA, $P < .01$ adjusted for multiple comparison using the FDR method). Expression of hCPT1AM in HFD-fed mice reverted the levels of 9 of these lipid species to what is seen in NCD-fed mice (shown in red in Figure 4B). Among them, we found that ceramide Cer (C20:0) was lower in the serum of HFD-hCPT1AM mice than in that of HFD-GFP control mice (Figure 4B). Several species of glycerophospholipids were also reduced in HFD-hCPT1AM serum, including phosphatidylcholines (PC (C34:1, C36:3, C36:4, and C38:6)), plasmalogen (pPC (C32:0)), and lysophosphatidylethanolamine (LPEA (C18:0)). Finally, only a few neutral lipids (DAG (C32:5) and TAG (C50:1)) showed significantly lower levels in the serum of HFD-hCPT1AM mice than in that of HFD-GFP control mice. As before, the clustering analysis was performed using complete linkage on the euclidean distances of the log-transformed values of the selected lipids. In this case, the analysis yielded three main clusters, and a fourth cluster containing a single animal (HFD-GFP 2), most likely an outlier. In general, the differences among groups were not as pronounced as those found when studying liver lipids, and the separation between HFD-hCPT1AM and HFD-GFP animals was not as definite (Figure 4B). Altogether, this comparative lipidomic analysis revealed that some lipid species (Cer (C20:0) and TAG (C50:1)) increase in the liver and serum of HFD-fed mice, yet, the expression of hCPT1AM in the liver is sufficient to partially or totally revert this increase both in the tissue and in serum (Figure 4C-D). Therefore, we hypothesized that these lipid species might be potential circulating biomarkers to monitor the amelioration of NAFLD during a therapeutic intervention.

3.7 | Serum lipidomic switch after bariatric surgery in obese humans

Lipidomic analyses in mice highlighted interesting potential biomarkers for monitoring human NAFLD. To determine the

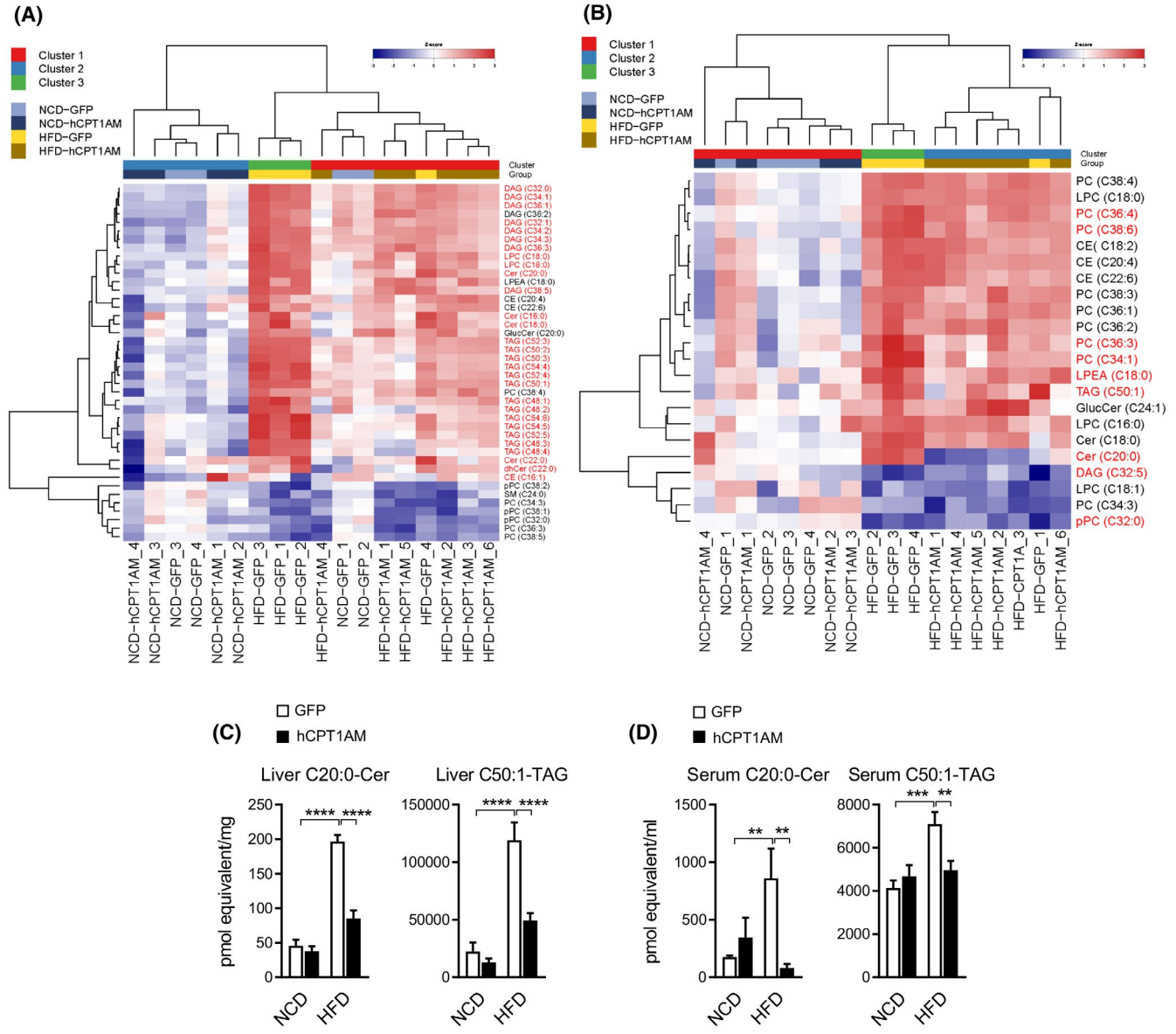

FIGURE 4 Lipidomic analyses of NCD- and HFD-fed mice after treatment with AAV9-GFP or AAV9-hCPT1AM. Lipidomic analyses of NCD- and HFD-fed mice after treatment with AAV9-GFP or AAV9-hCPT1AM. Unsupervised clustering of 18 mice (in columns) based on the quantification of (A) 42 lipids (in rows) in liver samples and (B) 24 lipids (in rows) in serum samples that exhibited statistically significant differences among NCD-GFP and HFD-GFP groups (two-way ANOVA $P < .01$ adjusted for multiple comparisons using FDR). The unsupervised clustering was performed using complete linkage on the Euclidean distance among samples. The heatmap colors represent the values scaled by the standard deviation of every lipid value across all samples and centered on the average of the NCD-GFP mice. Blue cells indicate values below the average value of the NCD-GFP mice, while red cells indicate values above that average, in z-scores. The lipid species highlighted in red exhibited statistically significant differences among HFD-GFP and HFD-hCPT1AM groups. Concentration of Cer (C20:0) and TAG (C50:1) (expressed in pmol equivalent) in liver (C) and serum (D) samples from NCD- and HFD-fed mice expressing either GFP or hCPT1AM (n = 4-6, $^{**}P < .01$, $^{***}P < .001$, $^{****}P < .0001$). Cer: ceramide; SM: sphingomyelin; GlucCer: glucosylceramide; PC: phosphatidylcholine; PE: phosphatidylethanolamine; PS: phosphatidylserine; DAG: diacylglycerol; TAG: triacylglycerol. Lipid species are annotated using the "lipid subclass" and "C followed by the total fatty acyl chain length:total number of unsaturated bonds" and (eg, PC (C32:2)). If the sphingoid base residue was dihydrosphingosine, the name contains a "dh" prefix. Plasmalogens and lysophospholipids are annotated as described above, except that a "p" or "L" prefix is included, respectively

clinical relevance of our findings, we performed a comparative serum lipidomic analysis of 15 lean control subjects and 15 obese patients, before and 6 months after Roux-en-Y gastric bypass (RYGB) (Table 2). Obese patients were diagnosed with NAFLD by liver biopsy (Table 3) and did not receive any antidiabetic treatment before surgery. The only patient on statin medication did not require lipid-lowering therapy 6 months after surgery. After RYGB, obese patients showed

TABLE 2 Clinical characteristics of the subjects included in the study

	Lean	Obese Pre-surgery	Obese Post-surgery	*P* (lean vs obese pre-surgery)	*P* (obese pre- vs post-surgery)
N	15	15	15	–	–
Sex (male/female)	4/11	4/11	4/11	.659	.659
Age (years)	42 ± 3	45 ± 3	46 ± 3	.470	**<.0001**
Height (m)	1.66 ± 0.02	1.64 ± 0.02	1.64 ± 0.02	.606	.334
Weight (kg)	63 ± 3	117 ± 6	79 ± 5	**<.00001**	**<.00001**
BMI (kg/m^2)	22.7 ± 0.8	43.0 ± 1.2	29.1 ± 1.0	**<.00001**	**<.00001**
Body fat (%)	28.7 ± 2.4	50.8 ± 1.3	36.1 ± 2.0	**<.00001**	**<.00001**
Waist circumference (cm)	80 ± 3	120 ± 4	95 ± 3	**<.00001**	**<.00001**
Glucose (mg/dL)	84 ± 2	104 ± 3	90 ± 8	**<.00001**	**<.00001**
Glucose 2-h OGTT (mg/dL)	95 ± 4	157 ± 8	-	**<.00001**	–
Insulin (μU/mL)	5.8 ± 0.9	19.2 ± 2.0	6.9 ± 1.0	**<.00001**	**<.00001**
Insulin 2-h OGTT (μU/mL)	44.9 ± 7.0	163.8 ± 24.4	-	**.002**	–
HOMA	1.2 ± 0.2	5.0 ± 0.6	1.6 ± 0.2	**<.00001**	**<.00001**
QUICKI	0.39 ± 0.01	0.31 ± 0.01	0.37 ± 0.01	**<.00001**	**<.00001**
Triacylglycerols (mg/dL)	78 ± 8	155 ± 17	83 ± 9	**<.00001**	**.002**
Total cholesterol (mg/dL)	192 ± 6	222 ± 9	165 ± 10	**.009**	.623
LDL-cholesterol (mg/dL)	109 ± 6	136 ± 8	102 ± 6	**.007**	**.041**
HDL-cholesterol (mg/dL)	68 ± 4	51 ± 5	54 ± 3	**.014**	**.050**
CRP (mg/L)	2.0 ± 0.6	10.2 ± 2.0	2.9 ± 0.9	**.003**	**.012**
Uric acid (mg/dL)	4.3 ± 0.2	6.2 ± 0.4	5.0 ± 0.4	**<.00001**	**.032**
Leptin (ng/mL)	11.0 ± 2.2	48.6 ± 6.3	12.7 ± 3.1	**<.00001**	**<.00001**
AST (IU/L)	13 ± 1	18 ± 2	15 ± 1	**.047**	.057
ALT (IU/L)	9 ± 1	29 ± 5	22 ± 5	**.001**	**<.00001**
Alkaline phosphatase (IU/L)	85 ± 4	100 ± 8	77 ± 10	.097	.132
γ-GT (IU/L)	12 ± 2	32 ± 9	17 ± 6	**.042**	**<.00001**
TSH (μU/mL)	1.7 ± 0.3	3.2 ± 1.3	–	.396	–
Daily alcohol intake (g)	2.1 ± 1.1	0.9 ± 0.7	–	.405	–
Antihypertensive therapy, n (%)	1 (6.7%)	6 (40.0%)	1 (6.7%)	.060	**.019**
Antidiabetic therapy, n (%)	0 (0%)	0 (0%)	0 (0%)	1.000	1.000
Lipid-lowering therapy, n (%)	0 (0%)	1 (6.7%)	0 (0%)	.536	.334

Note: Bold values denote statistically significant *P* values. Differences between lean subjects and patients with obesity before surgery were analyzed by Student's t test or χ^2 test, where appropriate. The impact of weight loss in patients with obesity before and 6 months after Roux-en-Y gastric bypass (RYGB) was analyzed by paired two-tailed Student's *t* test. n = 15.

Abbreviations: ALT, alanine aminotransferase; AST, aspartate aminotransferase; BMI, body mass index; CRP, high-sensitivity C-reactive protein; HOMA, homeostasis model assessment; IGT, impaired glucose tolerance; NG, normoglycemia; QUICKI, quantitative insulin sensitivity check index; T2D, type 2 diabetes; TSH, thyroid-stimulating hormone; γ-GT, γ-glutamyltransferase.

TABLE 3 Pathology analysis of liver biopsies obtained from patients with morbid obesity and NAFLD

Pathological characteristics	Obese NAFLD (%)
Steatosis	
<5%	27
5%-33%	53
34%-66%	13
>66%	7
Lobular inflammation	
No foci	33
<2 foci, per 200X field	13
2-4 foci, per 200X field	47
>4 foci, per 200X field	7
Portal inflammation	
None to minimal	27
Greater than minimal	73
Fibrosis stage	
None	60
Perisinusoidal or periportal/portal	13
Perisinusoidal and portal/periportal	20
Bridging fibrosis	7
Cirrhosis	0
Hepatocyte ballooning	
None	60
Few balloon cells	33
Many prominent balloon cells	7%
Mallory's hyaline	
None to rare	100
Many	0
Glycogenated nuclei	
None to rare	100
Many	0
Anatomopathological diagnosis	
NAFLD	60
NASH	40

lower weight and BMI (from 43.0 ± 1.2 to 29.1 ± 1 kg/m^2), decreased leptin levels and overall improved clinical biochemistry (Table 2). We analyzed 46 species of sphingolipids, 40 species of glycerophospholipids, and 50 species of neutral lipids (MAG, DAG, TAG, and cholesterol esters) by ESI-MS in serum from lean control subjects and obese patients before and after RYGB.

A subset of 26 lipids exhibited statistically significant differences among groups (ANOVA, $P < .01$ adjusted for multiple comparison using the FDR method) (Figure 5A). Unsupervised clustering analyses yielded three clusters with a very strong association with the sample type ($P = 2.2 \times$ 10-10, Chi-squared test). Notably Cluster 3, comprising most post-surgery individuals, was closer to Cluster 1 (mostly composed of lean control subjects) than to Cluster 2 (mostly obese pre-surgery individuals). These three clusters were not associated with gender ($P = .55$, Chi-squared test) or age ($P = .71$, ANOVA).

We also performed two complementary dimension reduction analyses, a classical principal component analysis (PCA) and a more sophisticated Uniform Manifold Approximation and Projection (UMAP), which is a nonlinear dimension reduction tool. In line with the results shown in Figure 4A, the dimension reduction analyses showed that the serum lipidomics values of the obese post-surgery patients were closer to those of lean controls than to the patients before surgery (Figure 5B). In the PCA, there was a very large difference in the first principal component mean value of obese pre-surgery patients with lean controls (difference = 10, P-adjusted = 4.7×10^{-7}) and obese post-surgery patients (difference = 9.2, P-adjusted = 4.6×10^{-6}), but not between lean and obese post-surgery patients (difference = 0.8, P-adjusted = .87). Similarly, the first dimension of the UMAP (UMAP 1) revealed a significant difference between obese pre-surgery individuals and lean controls (difference = 2.1, P-adjusted = 1.7×10^{-6}), as well as with obese post-surgery individuals (difference = 3.1, P-adjusted = 1.5×10^{-9}), but not between lean and obese post-surgery individuals (difference = 0.9, P-adjusted = 0.044).

Next, we evaluated the correlation between changes in serum lipid profiles and NAFLD variables, adjusting for changes in BMI. First, we calculated the serum lipid content change (ΔLC = content after surgery-content before surgery) and its correlation with BMI change (ΔBMI) in obese patients subjected to RYGB surgery. Fifty-five of the lipids analyzed exhibited statistically significant changes after surgery ($P < .05$, paired t test corrected for multiple comparisons), and only eight showed a significant correlation with changes in BMI ($P < .05$, correlation test corrected for multiple comparisons) (Figure 5C). Notably, there was no overlap between the set of lipids with significant changes after surgery and those that best correlated with changes in BMI. In general, lipids with larger ΔLC showed weak correlation with ΔBMI and, conversely, lipids whose ΔLC strongly correlated with ΔBMI had very modest ΔLC. This observation suggests that the most significant changes in serum lipid content do not directly reflect the loss of BMI.

When we compared the lipidomic analysis in mice serum and liver and human serum before and after therapeutic interventions such as AAV9-hCPT1AM administration and RYGB surgery, respectively, we noticed that TAG (C50:1) was increased in obese/NAFLD mice and humans but recovered after hCPT1AM expression in mice and RYGB surgery in humans (Figures 4D and 5D). As mentioned above, changes in TAG (C50:1) after bariatric surgery did

not correlate with changes in BMI. Therefore, the putative correlation of TAG and NAFLD score is likely to be independent. Unfortunately, some parameters for calculating the NAFLD score were not available. Nonetheless, we evaluated the association between ΔLC and NAFLD-related parameters, such as glucose levels, the AST/ALT ratio, GGT levels, ALT levels, and AST levels (Figure 5E), correcting for age, gender, and changes in BMI. As shown in Figure 5E, changes in TAG (C50:1) after bariatric surgery show a partial correlation with changes in NAFLD-related parameters. Altogether, these results highlight TAG (C50:1) as a potential circulating biomarker to monitor the amelioration of NAFLD during a therapeutic intervention.

4 | DISCUSSION

Here, we describe a partial reversion of an already established obese and diabetic phenotype through an enhanced FAO therapeutic intervention. AAVs have become a focus of attention in the field, especially in clinical-stage experimental therapeutic strategies, and are considered one of the safest strategies for gene therapy.[38] Two key factors of the present study are the use of the AAV9 serotype which efficiently and specifically targets hepatocytes and the use of the human isoform of CPT1AM (hCPT1AM) with the prospect of future clinical therapeutic applications. Thus, here we describe that AAV9-mediated hCPT1AM-expressing mice

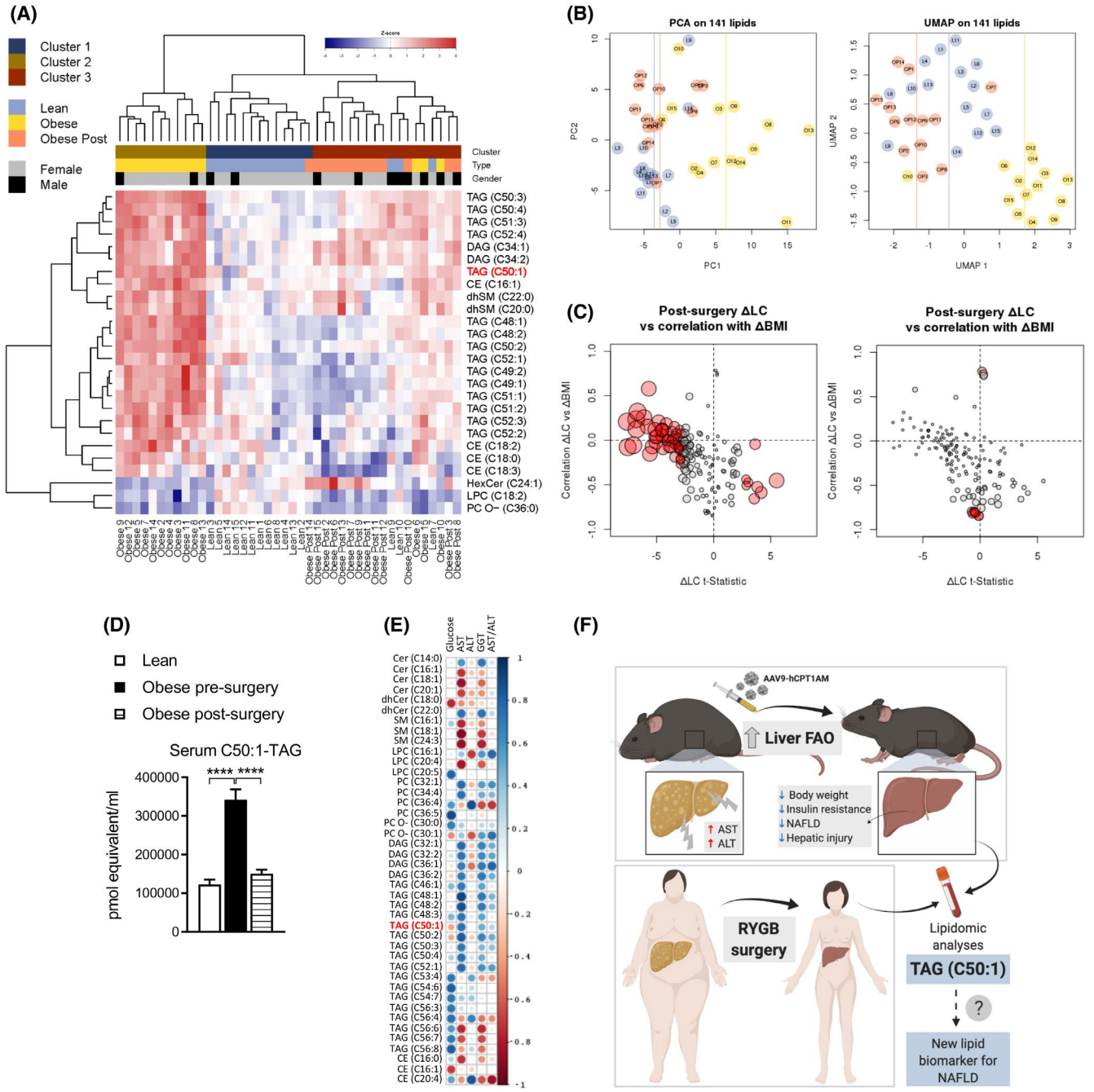

FIGURE 5 Lipidomic analyses in humans. A, Unsupervised clustering of 42 donors (in columns) based on the quantification of 26 lipids (in rows) that exhibited statistically significant differences among groups (ANOVA $P < .01$ adjusted for multiple comparisons using FDR). The unsupervised clustering was performed using complete linkage on the Euclidean distance among samples. The heatmap colors represents the values scaled by the standard deviation of every lipid values across all samples and centered on the average of the lean individuals. Blue cells indicate values below the average value of the lean individuals, while red cells indicate values above that average, in z-scores. B, (Left) Principal component analysis (PCA) of 42 donors based on the quantification of 141 lipids. To account for the large numerical differences among lipidic molecules, values were scaled to have unit variance before the PCA analysis. In blue, lean individuals (L); in yellow, obese patients pre-surgery (O); in orange the same patients post-surgery (OP). The vertical lines indicate the mean value on the first principal component (PC1, explaining around 27% of the total variance) for the three groups, using the same color code. (Right) Uniform manifold approximation and projection (UMAP) of the same data. Color code as in the figure on the left. C, (Left) Changes in serum lipid content (ΔLC, in x-axis) and its correlation with changes in BMI (y-axis). Every dot represents a lipid. ΔLC is the average difference in lipid content between pre- and post-surgery, measured in 12 patients with complete data. To account for large variability in the average value of different lipids, the t-Statistic values rather than the mean difference values are shown in the graph. Negative ΔLC t-Statistic values indicate lipids whose average value decreased after surgery. Conversely, positive values indicate lipids that increased after surgery. Dot sizes are proportional to the FDR-adjusted *P* value. In red, lipids with FDR-adjusted *P* value < .05. (Right) Same plot than on the left, but dot sizes are proportional to the FDR-adjusted *P* value of the correlation test. In red, those with FDR-adjusted *P* value < .05. D, Concentration of TAG (C50:1) (expressed in pmol equivalent) in sera samples from lean controls and obese patients before and after bariatric surgery (N = 15, ****$P < .0001$). E, Partial correlations of changes in lipid content with changes in NAFLD-related parameters, after selecting lipids that exhibited at least one of the five partial correlations with a *P* value < .05 (dot size is proportional to the magnitude of the correlation. In red, negative partial correlations. In blue positive partial correlations). F, Schematic representation of how AAV9-hCPT1AM reverses obesity-induced hepatic steatosis and the lipidomic strategy followed to identify TAG (C50:1) as a possible circulating biomarker for NAFLD. Cer: ceramide; SM: sphingomyelin; HexCer: hexosylceramides; PC, phosphatidylcholine; LPC: lysophosphatidylcholine; PE: phosphatidylethanolamine; LPEA: lysophosphatidylethanolamine; PC O-: ether-linked phosphatidylcholine; DAG: diacylglycerol; TAG: triacylglycerol; CE: cholesterol ester. Lipid species are annotated using the "lipid subclass" and "C followed by the total fatty acyl chain length:total number of unsaturated bonds" and (eg, PC (C32:2))

under HFD showed increased liver FAO and, importantly, reduced NAFLD and improved glucose tolerance and hepatic insulin signaling compared to HFD-fed control mice. In addition, hepatic hCPT1AM-expression in HFD-fed mice is sufficient to reduce potentially toxic lipid intermediates in the liver, such as DAG and ceramides, that can activate protein kinase C (PKCε) resulting in an impairment in the insulin signaling pathway.[39–42] These reduced ceramides and DAGs levels could explain the enhanced hepatic insulin signaling observed in HFD-hCPT1AM mice. Notably, hCPT1AM expression in NCD-fed mice did not significantly affect the hepatic and metabolic endpoints that were examined.

The expression of hCPT1AM does not have any noticeable deleterious effect in the liver, yet, it reverses hepatic injury as indicated by the lower serum levels of AST and ALT enzymes observed in HFD-hCPT1AM mice. However, it has been suggested that excessive FAO in muscle might lead to mitochondria overload and cell toxicity.[43] Here, we show that in HFD-hCPT1AM mice, three mechanisms could prevent possible oxidative stress caused by the accumulation of FAO metabolites in the mitochondria. First, the surplus of acetyl-CoA generated from FAO activates the ketogenic pathway. Second, part of the acetyl-CoA enters the TCA cycle for complete oxidation and ATP synthesis. Third, part of the energy produced is dissipated as heat. Nonetheless, the parallel increase in mitochondrial uncoupled and coupled respiration observed after hCPT1AM expression might seem paradoxical. One possible explanation could lie in previous reports showing that mild uncoupling, caused by activation of UCP2, might attenuate mitochondrial ROS production and protect against ROS-related cellular damage.[44-48] We hypothesized that an increase in mitochondrial FAs import in HFD-hCPT1AM mice might trigger a mild uncoupling intended to mitigate ROS production.

We examined the molecular mechanisms underlying the beneficial effects of hCPT1AM expression. Autophagy and lipolysis are two pathways implicated in the mobilization of lipid droplets (LDs) that are compromised after the onset of T2D and in genetic and diet-induced models of obesity.[36,49–52] In HFD-hCPT1AM mice, increased FAO results in a remarkable reduction of hepatic LDs. Consistently, levels of the structural proteins PLIN2 and PLIN5 were also low in HFD-hCPT1AM mice. However, protein analyses indicated that expression of hCPT1AM does not result in the activation of LD-associated lipases. Instead, the autophagy pathway appears to be activated in the liver of HFD-hCPT1AM mice. Importantly, recent studies have revealed a role for autophagy in hepatic LD breakdown.[37] Here, we propose that this mechanism could contribute to the reduction of hepatic lipid stores in HFD-hCPT1AM mice.

HFD-hCPT1AM mice showed lower levels of serum LDL-cholesterol than HFD-GFP controls. Given that one of the main determinants of VLDL synthesis is hepatic TAG content, which is significantly reduced in HFD-hCPT1AM mice, we speculate that secretion of VLDL might be reduced in HFD hCPT1AM-expressing mice. Consequently, the derived LDL levels are lower. Moreover, hCPT1AM expression in the liver restored some aspects of cholesterol metabolism,

such as protein levels of lipoprotein transporters and mRNA levels of cholesterol transporters.

There is great interest in finding new circulating biomarkers for NAFLD/NASH diagnosis and monitoring of treatment effectiveness. While some studies have analyzed specific lipid profiles in models of NAFLD, obesity, and T2D,[53–55] only a few studies have focused on changes of lipid species in liver and serum under interventions that improve hepatic steatosis and obesity. Here, we performed a comparative lipidomic analyses in mice and humans that aimed to look for potential noninvasive markers to monitor the progression of NAFLD in pathological conditions (ie, obesity) before and after therapeutic interventions intended to reduce body weight and hepatic steatosis (ie, AAV9-mediated hCPT1AM expression in mice and Roux-en-Y gastric bypass in humans). In mice, our results show that TAG with a longer, unsaturated chain of FAs (TAG (C50:1/2/3), TAG (C52:3/4/5), and TAG (C54:1/4/5/6)) increased in the liver of HFD-fed mice. However, the expression of hCPT1AM decreases the concentration of these lipid species back to what is seen in NCD-fed mice. Interestingly, one of these species, TAG (C50:1), follows the same pattern in the serum of HFD-hCPT1AM, which suggests that this TAG could be a circulating biomarker of hepatic steatosis. These results are in line with a previous study showing that treatment of HFD-fed mice with compound K-enriched with ginsenosides, which decreases hepatic steatosis in treated mice, also reduced serum levels of TAG species with a total number of carbons above 50.[56]

Remarkably, in the serum of patients with obesity and NAFLD, similar TAG species (TAG (C50:1/2/3) and TAG (C52:3/4)) are reduced 6 months after bariatric surgery. These results are in line with previous studies reporting a reduction in TAG (C50:1), among other TAGs, in plasma/serum of obese patients after RYGB interventions.[57,58] Conceivably the mechanisms behind TAG changes might be different in humans and in hCPT1AM-expressing mice. In HFD-hCPT1AM mice the increase in hepatic FAO mobilizes stored lipid droplets and reduces the number of substrates for hepatic TAG synthesis. In humans, we can speculate that decreased intestinal fat absorption and altered hormone levels might reduce hepatic lipid accumulation. In our study, changes in many of these lipid content in the serum of obese patients after bariatric surgery correlate with changes in NAFLD-related parameters and do not directly reflect the loss of BMI. Yet, the decrease in circulating TAG (C50:1) after RYGB could be mediated by other parameters beyond hepatic steatosis. Nonetheless, our results in mice and human samples support speculation on its possible role as a noninvasive biomarker for human NAFLD diagnosis and prognosis. Additionally, we cannot reject the possibility that other circulating lipid species that changed in our human intervention study, as well as in other published paper [57–59] could be circulating biomarkers for NAFLD. It is important to note that our study did not investigate the role of CPT1A in human NAFLD or in the observed changes in serum lipidomic profiles after RYGB. Nonetheless, previous reports have shown that liver CPT1A expression is remarkably decreased in biopsy samples from NAFLD patients.[60,61] This observation indicates that decreased β-oxidation in human NAFLD could contribute to fatty acid accumulation in hepatocytes. This suggests that our preclinical observations in mice could be relevant for future human research. Overall, the strength of our lipidomic study is based on the comparison of mice and human samples of hepatic steatosis, before and after therapeutic intervention. This strategy allows us to look for specific, robust serum biomarkers that reflect the progression of NAFLD and the effectiveness of a therapeutic intervention. In the future, the hypothesized candidate biomarker should be validated in a larger cohort of participants before it is used for clinical purposes.

In summary, here we report an efficient gene therapy approach to greatly reduce liver steatosis and body weight and to improve glucose tolerance and hepatic insulin signaling in a mouse model of HFD-induced obesity (Figure 5F). Moreover, we shed light on the molecular mechanisms involved in the beneficial effects of increasing FAO in hepatocytes. Finally, based on a comparative lipidomic analysis of mouse and human samples, we hypothesize a candidate circulating biomarker to monitor obesity and hepatic steatosis and the effectiveness of therapeutic interventions (Figure 5F). The future directions of this work should include long-term experiments (1 year or more) in mice, rats, and higher animal species (monkeys) to ratify the effectiveness of the gene therapy and identify potential long-term side effects or cytotoxicity. Moreover, studies in larger human cohorts would confirm the prospective clinical applicability of the suggested circulating biomarker. Altogether, our results point toward the human isoform of CPT1A as a potential therapeutic target against NAFLD and obesity-induced disorders.

ACKNOWLEDGMENTS

We thank Gloria González-Aseguinolaza for kindly supplying the EalbAATp promoter. Financial support statement: This study was supported by the Ministry of Spain (MINECO) (SAF2014-52223-C2-1-R to DS, SAF2017-83813-C3-1-R to DS and LH, SAF2017-82813-C3-3R to NC co-financed by the European Regional Development Fund [ERDF], a doctoral fellowship to JFM, and a Juan de la Cierva—Incorporación research fellowship [IJCI-2016-28313] to PM and DS), the Centro de Investigación Biomédica en Red de Fisiopatología de la Obesidad y la Nutrición (CIBEROBN) (CB06/03/0001 to DS), the Government of Catalonia (2014SGR465 to DS), Instituto de Salud Carlos III (FISPI18/01584 to VL-C, FIS-PI17/00412 to RB, FIS PI18/01484 to SA and FIS17/01455 to DS-I, Miguel Servet Fund CP15/00106 to DS-I and Rio

Hortega grant (CM19/00039) to CM) and co-financed by the European Regional Development Fund (ERDF), Centro de Investigación Biomédica en Red de Diabetes y Enfermedades Metabólicas Asociadas (CIBERDEM) to JC-EG, the Fundació La Marató de TV3 (201627-30 to DS and 201627-31 to NC), the European Foundation for the Study of Diabetes (EFSD)/Lilly and EFSD/Janssen-Rising Star and L'Oréal-UNESCO "For Women in Science" research fellowships to LH, a doctoral fellowship from the Ciência sem Fronteiras-CNPq (237976/2012-9) to MW. Figure 4F was created with BioRender.com.

CONFLICT OF INTEREST

The material reported in this manuscript is original and has not been previously published or submitted for publication elsewhere. All authors approve the manuscript and declare no conflict of interest.

AUTHOR CONTRIBUTIONS

M. Weber, P. Mera, R. Bartrons, A. Zorzano, V. Llorente-Cortes, G. Frühbeck, N. Casals, L. Herrero, and D. Serra designed research and conceptualized the study. M. Weber, P. Mera, F. Casas, D. Sebastián, M. C. Soler-Vázquez, S. Recalde, R. Fucho, M. Calderon-Dominguez, J. F. Mir, and J. C. Escola-Gil performed research. M. Weber, P. Mera, S. Alonso, and D. Sánchez-Infantes prepared images and graphical data. M. Weber, P. Mera, F. Casas, A. Rodríguez, S. Alonso, J. C. Escola-Gil, and D. Sánchez-Infantes analyzed data. P. Mera, L. Herrero, and D. Serra wrote the paper. J. Salvador, A. Rodríguez, G. Frühbeck, and V. Valentí contributed clinical samples. Supervision, project administration, and funding acquisition: L. Herrero, D. Serra. P. Mera, L. Herrero, and D. Serra had primary responsibility for final content. All authors read and approved the final manuscript.

REFERENCES

1. Younossi ZM, Koenig AB, Abdelatif D, Fazel Y, Henry L, Wymer M. Global epidemiology of nonalcoholic fatty liver disease-Meta-analytic assessment of prevalence, incidence, and outcomes. *Hepatology*. 2016;64:73-84.
2. Abu-Elheiga L, Oh W, Kordari P, Wakil SJ. Acetyl-CoA carboxylase 2 mutant mice are protected against obesity and diabetes induced by high-fat/high-carbohydrate diets. *Proc Natl Acad Sci USA*. 2003;100:10207-10212.
3. An J, Muoio DM, Shiota M, et al. Hepatic expression of malonyl-CoA decarboxylase reverses muscle, liver and whole-animal insulin resistance. *Nat Med*. 2004;10:268-274.
4. Ishigaki Y, Katagiri H, Yamada T, et al. Dissipating excess energy stored in the liver is a potential treatment strategy for diabetes associated with obesity. *Diabetes*. 2005;54:322-332.
5. Woods A, Williams JR, Muckett PJ, et al. Liver-specific activation of AMPK prevents steatosis on a high-fructose diet. *Cell Rep*. 2017;18:3043-3051.
6. Ferré P. The biology of peroxisome proliferator-activated receptors: relationship with lipid metabolism and insulin sensitivity. *Diabetes*. 2004;53(Suppl 1):S43-50.
7. Zhang D, Christianson J, Liu Z-X, et al. Resistance to high-fat diet-induced obesity and insulin resistance in mice with very long-chain acyl-CoA dehydrogenase deficiency. *Cell Metab*. 2010;11:402-411.
8. Stefanovic-Racic M, Perdomo G, Mantell BS, Sipula IJ, Brown NF, O'Doherty RM. A moderate increase in carnitine palmitoyltransferase 1a activity is sufficient to substantially reduce hepatic triglyceride levels. *Am J Physiol Endocrinol Metab*. 2008;294:E969-E977.
9. Morillas M, Gómez-Puertas P, Bentebibel A, et al. Identification of conserved amino acid residues in rat liver carnitine palmitoyltransferase I critical for malonyl-CoA inhibition. Mutation of methionine 593 abolishes malonyl-CoA inhibition. *J Biol Chem*. 2003;278:9058-9063.
10. Orellana-Gavaldà JM, Herrero L, Malandrino MI, et al. Molecular therapy for obesity and diabetes based on a long-term increase in hepatic fatty-acid oxidation. *Hepatology*. 2011;53:821-832.
11. Monsénégo J, Mansouri A, Akkaoui M, et al. Enhancing liver mitochondrial fatty acid oxidation capacity in obese mice improves insulin sensitivity independently of hepatic steatosis. *J Hepatol*. 2012;56:632-639.
12. Brunt EM. Nonalcoholic steatohepatitis. *Semin Liver Dis*. 2004;24:3-20.
13. Ezquerro S, Mocha F, Frühbeck G, et al. Ghrelin reduces TNF-α-induced human hepatocyte apoptosis, autophagy and pyroptosis: role in obesity-associated NAFLD. *J Clin Endocrinol Metab*. 2018;104(1):21-37. https://doi.org/10.1210/jc.2018-01171
14. Matthews DR, Hosker JP, Rudenski AS, Naylor BA, Treacher DF, Turner RC. Homeostasis model assessment: insulin resistance and β-cell function from fasting plasma glucose and insulin concentrations in man. *Diabetologia*. 1985;28(7):412-419.
15. Katz A, Nambi SS, Mather K, et al. Quantitative insulin sensitivity check index: a simple, accurate method for assessing insulin sensitivity in humans. *J Clin Endocrinol Metab*. 2000;85(7):2402-2410. https://doi.org/10.1210/jcem.85.7.6661
16. Kramer MG, Barajas M, Razquin N, et al. In vitro and in vivo comparative study of chimeric liver-specific promoters. *Mol Ther*. 2003;7:375-385.
17. Donello JE, Loeb JE, Hope TJ. Woodchuck hepatitis virus contains a tripartite posttranscriptional regulatory element. *J Virol*. 1998;72:5085-5092.
18. Fraser F, Corstorphine CG, Zammit VA. Topology of carnitine palmitoyltransferase I in the mitochondrial outer membrane. *Biochem J*. 1997;323:711-718.
19. Lee K, Kerner J, Hoppel CL. Mitochondrial carnitine palmitoyltransferase 1a (CPT1a) is part of an outer membrane fatty acid transfer complex. *J Biol Chem*. 2011;286:25655-25662.
20. Morillas M, Gómez-Puertas P, Roca R, et al. Structural model of the catalytic core of carnitine palmitoyltransferase I and carnitine octanoyltransferase (COT): Mutation of CPT I histidine 473 and alanine 381 and COT alanine 238 impairs the catalytic activity. *J Biol Chem*. 2001;276:45001-45008.
21. Dentin R, Pégorier J-P, Benhamed F, et al. Hepatic glucokinase is required for the synergistic action of ChREBP and SREBP-1c on glycolytic and lipogenic gene expression. *J Biol Chem*. 2004;279:20314-20326.

22. Veerkamp JH, van Moerkerk TB, Glatz JF, Zuurveld JG, Jacobs AE, Wagenmakers AJ. 14CO2 production is no adequate measure of [14C]fatty acid oxidation. *Biochem Med Metab Biol*. 1986;35:248-259.
23. Morillas M, Clotet J, Rubí B, et al. Identification of the two histidine residues responsible for the inhibition by malonyl-CoA in peroxisomal carnitine octanoyltransferase from rat liver. *FEBS*. 2000;Lett:466.
24. Escolà-Gil JC, Llaverias G, Julve J, Jauhiainen M, Méndez-González J, Blanco-Vaca F. The cholesterol content of western diets plays a major role in the paradoxical increase in high-density lipoprotein cholesterol and upregulates the macrophage reverse cholesterol transport pathway. *Arterioscler Thromb Vasc Biol*. 2011;31:2493-2499.
25. Martínez-Sánchez N, Seoane-Collazo P, Contreras C, et al. Hypothalamic AMPK-ER stress-JNK1 axis mediates the central actions of thyroid hormones on energy balance. *Cell Metab*. 2017;26:212-229.e12.
26. R: A language and environment for statistical computing.
27. Ritchie ME, Phipson B, Wu D, et al. Limma powers differential expression analyses for RNA-sequencing and microarray studies. *Nucleic Acids Res*. 2015;43:e47.
28. Shilin Zhao A, Yin L, Guo Y, Sheng Q, Shyr Maintainer Shilin Zhao Y. Package "heatmap3" Type Package Title An Improved Heatmap Package; 2019.
29. McInnes, L., John Healy, J., Melville, J. (2018)UMAP: Uniform Manifold Approximation and Projection for Dimension Reduction. *arXiv e-prints*: 1802.03426
30. McInnes L, Healy J, Saul N, Großberger L. UMAP: uniform manifold approximation and projection. *J Open Source Software*. 2018;3(29):861. https://doi.org/10.21105/joss.00861
31. Kim S. ppcor: an R package for a fast calculation to semi-partial correlation coefficients. *Commun Stat Appl Methods*. 2015;22:665-674.
32. Wei T, Simko V. R package "corrplot": visualization of a correlation matrix (Version 0.84); 2017. https://github.com/taiyun/corrplot
33. Benjamini Y, Hochberg Y. Benjamini-1995.pdf. *J R Stat Soc B*. 1995;57:289-300.
34. Kleiner DE, Brunt EM, Van Natta M, et al. Design and validation of a histological scoring system for nonalcoholic fatty liver disease. *Hepatology*. 2005;41:1313-1321.
35. Kimmel AR, Sztalryd C. The Perilipins: major cytosolic lipid droplet-associated proteins and their roles in cellular lipid storage, mobilization, and systemic homeostasis. *Annu Rev Nutr*. 2016;36:471-509.
36. Singh R, Cuervo AM. Lipophagy: connecting autophagy and lipid metabolism. *Int J Cell Biol*. 2012;2012:1-12.
37. Singh R, Kaushik S, Wang Y, et al. Autophagy regulates lipid metabolism. *Nature*. 2009;458:1131-1135.
38. Naso MF, Tomkowicz B, Perry WL, Strohl WR. Adeno-Associated Virus (AAV) as a vector for gene therapy. *BioDrugs*. 2017;31:317-334.
39. Gassaway BM, Petersen MC, Surovtseva YV, et al. PKCε contributes to lipid-induced insulin resistance through cross talk with p70S6K and through previously unknown regulators of insulin signaling. *Proc Natl Acad Sci*. 2018;115:E8996-E9005.
40. Samuel VT, Petersen MC, Gassaway BM, Vatner DF, Rinehart J, Shulman GI. Considering the links between nonalcoholic fatty liver disease and insulin resistance: revisiting the role of protein Kinase C ε. *Hepatology*. 2019;70(6):2217-2220. https://doi.org/10.1002/hep.30829
41. Turinsky J, O'Sullivan DM, Bayly BP. 1,2-Diacylglycerol and ceramide levels in insulin-resistant tissues of the rat in vivo. *J Biol Chem*. 1990;265:16880-16885.
42. Ussher JR, Koves TR, Cadete VJJ, et al. Inhibition of De Novo ceramide synthesis reverses diet-induced insulin resistance and enhances whole-body oxygen consumption. *Diabetes*. 2010;59(10):2453-2464. https://doi.org/10.2337/db09-1293
43. Koves TR, Ussher JR, Noland RC, et al. Mitochondrial overload and incomplete fatty acid oxidation contribute to skeletal muscle insulin resistance. *Cell Metab*. 2008;7(1):45-56. https://doi.org/10.1016/j.cmet.2007.10.013
44. Skulachev VP. Role of uncoupled and non-coupled oxidations in maintenance of safely low levels of oxygen and its one-electron reductants. *Q Rev Biophys*. 1996;29:169-202.
45. Nègre-Salvayre A, Hirtz C, Carrera G, et al. A role for uncoupling protein-2 as a regulator of mitochondrial hydrogen peroxide generation. *FASEB J*. 1997;11:809-815.
46. Echtay KS, Roussel D, St-Plerre J, et al. Superoxide activates mitochondrial uncoupling proteins. *Nature*. 2002;415:96-99.
47. Cortez-Pinto H, Zhi Lin H, Qi Yang S, Odwin Da Costa S, Diehl AM. Lipids up-regulate uncoupling protein 2 expression in rat hepatocytes. *Gastroenterology*. 1999;116:1184-1193.
48. Casteilla L, Rigoulet M, Pénicaud L. Mitochondrial ROS metabolism: modulation by uncoupling proteins. *IUBMB Life*. 2001;52:181-188.
49. Yang L, Li P, Fu S, Calay ES, Hotamisligil GS. Defective hepatic autophagy in obesity promotes ER stress and causes insulin resistance. *Cell Metab*. 2010;11:467-478.
50. Martinez-Lopez N, Singh R. Autophagy and Lipid Droplets in the Liver. *Annu Re Nutr*. 2015;35:215-237.
51. Ezquerro S, Mocha F, Frühbeck G, et al. Ghrelin reduces TNF-α-induced human hepatocyte apoptosis, autophagy and pyroptosis: role in obesity-associated NAFLD. *J Clin Endocrinol Metab*. 2018;104:21-37.
52. Alexaki A, Gupta SD, Majumder S, et al. Autophagy regulates sphingolipid levels in the liver. *J Lipid Res*. 2014;55:2521-2531.
53. Puri P, Baillie RA, Wiest MM, et al. A lipidomic analysis of nonalcoholic fatty liver disease. *Hepatology*. 2007;46:1081-1090.
54. Sanyal AJ, Pacana T. A lipidomic readout of disease progression in a diet-induced mouse model of nonalcoholic fatty liver disease. *Trans Am ClinClimatol Assoc*. 2015;126:271-288.
55. Kahle M, Schäfer A, Seelig A, et al. High fat diet-induced modifications in membrane lipid and mitochondrial-membrane protein signatures precede the development of hepatic insulin resistance in mice. *Mol Metab*. 2014;4:39-50.
56. Shon JC, Shin H-S, Seo YK, Yoon Y-R, Shin H, Liu K-H. Direct infusion MS-based lipid profiling reveals the pharmacological effects of compound K-reinforced ginsenosides in high-fat diet induced obese mice. *J Agric Food Chem*. 2015;63:2919-2929.
57. Graessler J, Bornstein TD, Goel D, et al. Lipidomic profiling before and after Roux-en-Y gastric bypass in obese patients with diabetes. *Pharmacogenomics J*. 2014;14:201-207.
58. Velagapudi V, Welbourn R, Arora T, et al. Roux-en-Y gastric bypass surgery induces early plasma metabolomic and lipidomic alterations in humans associated with diabetes remission. *PLoS One*. 2015;10:e0126401.

59. Kayser BD, Lhomme M, Dao MC, et al. Serum lipidomics reveals early differential effects of gastric bypass compared with banding on phospholipids and sphingolipids independent of differences in weight loss. *Int J Obes*. 2017;41:917-925.
60. Kohjima M, Enjoji M, Higuchi N, et al. Re-evaluation of fatty acid metabolism-related gene expression in nonalcoholic fatty liver disease. *Int J Mol Med*. 2007;20(3):351-358. https://doi.org/10.3892/ijmm.20.3.351
61. Nakamuta M, Kohjima M, Morizono S, et al. Evaluation of fatty acid metabolism-related gene expression in nonalcoholic fatty liver disease. *Int J Mol Med*. 2005;16:631-635.

SUPPORTING INFORMATION

Additional Supporting Information may be found online in the Supporting Information section.

How to cite this article: Weber M, Mera P, Casas F, et al. Liver CPT1A gene therapy reduces diet-induced hepatic steatosis in mice and highlights potential lipid biomarkers for human NAFLD. *The FASEB Journal*. 2020;34:11816–11837. https://doi.org/10.1096/fj.202000678R